Cell Reports
Medicine

Article

CD97 maintains tumorigenicity of glioblastoma stem cells via mTORC2 signaling and is targeted by CAR Th9 cells

Graphical abstract

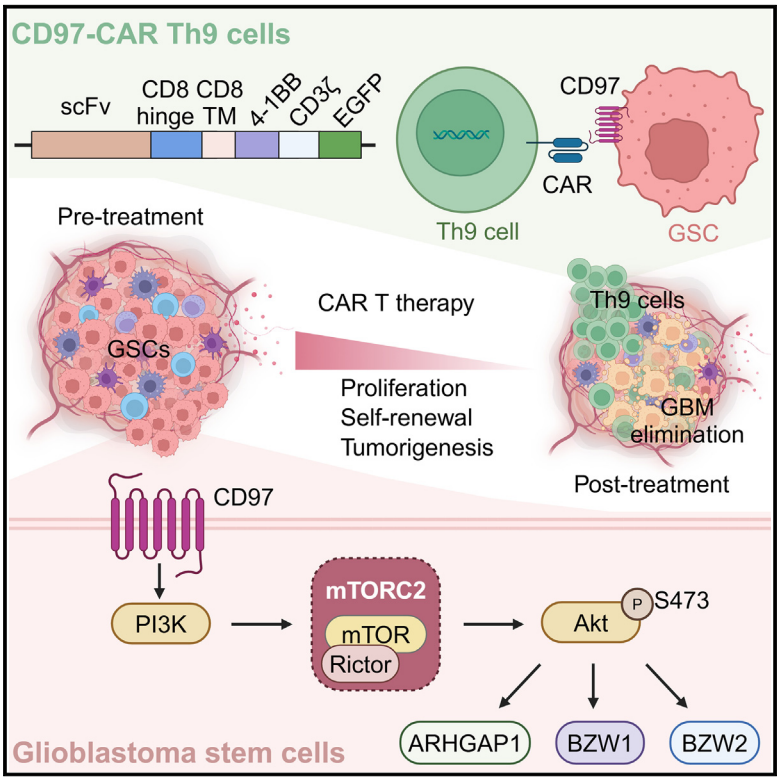

Highlights

- *In vitro* antibody screening identified CD97 as an optimal GSC surface antigen
- CD97 strongly correlates with intracellular GSC markers
- CD97 regulates ARHGAP1, BZW1, and BZW2 expression via mTORC2-AKT signaling
- CD97-targeting CAR Th9 cells show a potent antitumor response

Authors

Shuchang Zhou, Weiwei Lin, Xiong Jin, ..., Sun Il Choi, Bingyang Shi, Jinlong Yin

Correspondence

jlyin@henu.edu.cn (J.Y.),
bs@henu.edu.cn (B.S.),
sunil.choi@hotmail.com (S.I.C.)

In brief

Zhou et al. identify CD97 as a regulator of GSC maintenance via mTORC2 signaling activation. Targeting CD97 with CAR Th9 cells exhibits potent cytotoxic effects and prolongs survival in mice, highlighting CD97 as a promising antigen for GBM-targeted therapy.

Zhou et al., 2024, Cell Reports Medicine *5*, 101844
December 17, 2024
https://doi.org/10.1016/j.xcrm.2024.101844

CellPress

Cell Reports Medicine

CellPress
OPEN ACCESS

Article

CD97 maintains tumorigenicity of glioblastoma stem cells via mTORC2 signaling and is targeted by CAR Th9 cells

Shuchang Zhou,[1,2,7] Weiwei Lin,[3,4,7] Xiong Jin,[1,5,7] Rui Niu,[1,2] Zheng Yuan,[1,2] Tianran Chai,[1,2,6] Qi Zhang,[1,2] Meixia Guo,[1,2] Sung Soo Kim,[6] Meichen Liu,[1,2,6] Yilin Deng,[1,2,6] Jong Bae Park,[4,6] Sun Il Choi,[1,5,*] Bingyang Shi,[1,2,*] and Jinlong Yin[1,2,8,*]

[1]The Zhongzhou Laboratory for Integrative Biology, Henan Key Laboratory of Brain Targeted Bio-Nanomedicine, School of Life Sciences, Henan University, Kaifeng, Henan 475004, China

[2]Henan-Macquarie University Joint Centre for Biomedical Innovation, School of Life Sciences, Henan University, Kaifeng, Henan 475004, China

[3]Henan Institute of Medical and Pharmaceutical Sciences, Zhengzhou University, Zhengzhou, Henan 450052, China

[4]Research Institute, National Cancer Center, Goyang, Gyeonggi 10408, Republic of Korea

[5]School of Pharmacy, Henan University, Kaifeng, Henan 475004, China

[6]Cancer Biomedical Science, Graduate School of Cancer Science and Policy, National Cancer Center, Goyang 10408, Republic of Korea

[7]These authors contributed equally

[8]Lead contact

*Correspondence: jlyin@henu.edu.cn (J.Y.), bs@henu.edu.cn (B.S.), sunil.choi@hotmail.com (S.I.C.)

https://doi.org/10.1016/j.xcrm.2024.101844

SUMMARY

Glioblastoma (GBM) stem cells (GSCs) contribute to poor prognosis in patients with GBM. Identifying molecular markers is crucial for developing targeted therapies. Here, we identify cluster of differentiation 97 (CD97) as an optimal GSC surface antigen for potential targeting by chimeric antigen receptor (CAR) T cell therapy through *in vitro* antibody screening. CD97 is consistently expressed in all validated patient-derived GSCs and positively correlated with known intracellular GSC markers. Silencing CD97 reduces GSC tumorigenicity-related activities, including self-renewal, proliferation, and tumor progression. Transcriptome analysis reveals that CD97 activates mTORC2, leading to AKT S473 phosphorylation and enhanced expression of the downstream genes *ARHGAP1*, *BZW1*, and *BZW2*. Inhibiting mTORC2 with JR-AB2-011 suppresses GSC tumorigenicity and downstream gene expression. We develop CD97-CAR T helper (Th) 9 cells, which exhibit potent cytotoxic effects *in vitro* and extend survival in mice. These findings suggest that CD97 is a promising GSC-enriched antigen and that targeting it with CAR Th9 cells offers a potential therapeutic strategy for GBM.

INTRODUCTION

Glioblastoma (GBM) is the most common malignant primary brain tumor with a median overall survival of 14–16 months despite intensive treatment.[1,2] One of the leading causes of GBM aggressiveness, high recurrence, and resistance to therapy is cancer heterogeneity, especially GBM stem cells (GSCs).[3] GSCs are subpopulations of cells capable of initiating tumor progression to organize proliferation and produce pathognomonic heterogeneity and more differentiated cancer cells.[3] Identification and validation of a molecular marker of GSCs are important to classify tumor cell features and translate them into GSC-targeted therapies. However, potential GSC-targeted therapies, especially chimeric antigen receptor (CAR) T cell therapy, are not yet well established due to the current lack of reliable tumor antigens for targeting.

The success of Food and Drug Administration approval for CD19-CAR T cells as a treatment for B cell malignancies[4] has greatly encouraged researchers to develop CAR T therapy for patients with GBM. However, early clinical outcomes with CAR T cells targeting IL-13 receptor α chain 2,[5] epidermal growth factor receptor variant III,[6] and human epidermal growth factor receptor 2[7] were limited. Therefore, studies are urgently needed to discover reliable GSC-specific surface antigens and reveal the functions of recognized antigens to develop GSC-targeted CAR T cells. Although several surface markers have been identified for GSCs, such as CD133,[8–10] CD44,[11,12] CD15,[13,14] CD9,[15] L1CAM,[16] CD321,[17] and CD49f,[18] their potency in CAR development is limited due to their expression in normal neural stem cells or astrocytes. A recent study suggested the rational development of CD133-targeting immunotherapies, including CD133-targeting CAR T cells for GBM and brain metastasis,[19,20] but the use of CD133 as a specific surface antigen of GSCs is controversial.[19] Following in-depth research, a large number of studies demonstrated that CD133-negative cells also form brain tumors.[21] Moreover, the cell surface antigens having a biological function in regulating GSC maintenance and tumorigenesis are restricted, and the potency for developing antitumor CAR T cells is challenged.

Here, we used a human surface protein antibody array and found that all validated patient-derived GSCs uniformly and

specifically express the surface antigen cluster of differentiation 97 (CD97). CD97 showed a remarkable presence on GSCs and was associated with adverse outcomes in patients with GBM. It showed a strong positive association with intracellular GSC markers, such as Nestin, Oct3/4, and Nanog, suggesting its suitability as an exclusive surface marker for GSCs. Functionally, CD97 activates mTORC2-AKT signaling to maintain the tumorigenicity of GSCs. Furthermore, CD97^{high} GSCs promote aggressive tumor growth *in vitro* and *in vivo* and confer a poor prognosis to patients with GBM. Finally, we developed CD97-targeting CAR T helper (Th) 9 cells and showed a potential antitumor response against GBM. Collectively, these findings suggest that CD97 is a functional GSC surface antigen, and CD97-targeting CAR Th9 cell therapy may be a potent strategy for treatment-refractory GBM.

RESULTS

Identification of CD97 as a potential surface antigen for GSCs

To identify a generally optimal enriched surface antigen of GSCs, we first screened GSCs (83 and X01), serum-induced differentiated GSCs (X01-Diff), and normal astrocytes (Ast) using commercially available cell surface protein antibody panels (Figure 1A). The antibody array generated data for 242 human cell surface proteins and 9 isotype controls. The percentage of positive cells was determined for each cell surface protein using a high-throughput confocal imaging system, and values from replicates were averaged. We identified potential GSC surface antigens based on the following three criteria: (1) the candidate was not or minimally expressed in Ast, (2) the candidate was expressed with high levels in 83 and X01 GSCs, and (3) the candidate showed compromised expression levels in differentiated GSCs. Thus, we identified CD97 as our top candidate (Figure 1B). The characterization of CD97 as a potential surface antigen of GSCs is shown in the representative confocal immunofluorescence (IF) micrographs and the accompanying quantitative evaluation (Figures 1C and 1D).

CD97, which is encoded by the gene *ADGRE5*, is a member of the epidermal growth factor subfamily of the adhesion G protein-coupled receptor class of cell surface proteins.[22] CD97 was first reported to be involved in cell proliferation, adhesion, and migration in different immunophenotypes of diseases.[22] Recent studies have implicated abundant CD97 expression detected in acute myeloid leukemia,[23] thyroid,[24] hepatocellular,[25] colorectal,[26] and pancreatic cancers,[27] as well as GBM.[28–37] Functionally, CD97 has been shown not only to confer cell adhesion through interaction with other extracellular matrix proteins but also to stimulate angiogenesis and induce cancer invasion. However, its association with GBM, particularly in GSC biology, has yet to be thoroughly investigated. Consistent with the expression profiles obtained from antibody screening, the CD97 mRNA and protein were expressed at high levels in GSCs, and CD97 expression was noticeably decreased after GSC differentiation (Figure 1E). CD97 was further validated as a hit using flow cytometry, and a high expression level of CD97 was detected in 83 and X01, and its expression was markedly decreased in GSCs under serum-induced differentiation conditions (Figure 1F). We evaluated eight additional patient-derived GSCs (131, 528, 448, GSC772, GSC211, GSC924, GSC028, and GSC428) using flow cytometry to further confirm these findings in a wider range of GSCs, and CD97 was ubiquitously overexpressed in all tested GSCs (Figure 1G). Collectively, these data suggest that CD97 could be an ideal GSC surface antigen.

CD97 is correlated with a poor prognosis for patients with GBM

Subsequently, to investigate the clinical relevance of CD97 in patients with GBM, we performed an *in silico* analysis utilizing publicly available glioma datasets. Higher levels of CD97 protein abundance were observed in patients with GBM than in nontumor tissues from the Clinical Proteomic Tumor Analysis Consortium cohort (CPTAC)[38] (Figure 1H). Additionally, CD97 was expressed at high levels in all three GBM subtypes, which were classified based on different molecular signatures (Figure 1I).[39] Notably, upregulated CD97 protein expression was also associated with a poor prognosis for those patients (Figure 1J). These findings were consistent with the results using mRNA glioma datasets from The Cancer Genome Atlas (TCGA), the Chinese Glioma Genome Atlas (CGGA), and the Repository of Molecular Brain Neoplasia Data (REMBRANDT) (Figure S1). These results strongly indicate that high expression of CD97, either in protein or mRNA level, is remarkably correlated with worse outcomes for patients with GBM.

CD97 identifies the GSC population and maintains GSC tumorigenicity

To determine the role of CD97 as an optimal surface antigen in GSC identification, we performed a bioinformatics analysis. First, we interrogated single-cell RNA sequencing datasets using Restall[40] and Richards[41] cohorts and found evidence that ADGRE5/CD97 is highly expressed in GSCs (Figure 2A). Next, we calculated the Pearson correlation coefficient (R) between individual genes associated with conventional, well-known GSC markers (Nestin,[9,42] Sox2,[43] Nanog,[44] Oct3/4,[45] PROM1/CD133,[10] CD44,[11] FUT4/CD15,[13] and ITGA6/CD49f[18]) and ADGRE5/CD97 using public databases, including TCGA, CCGA, REMBRANDT, and CPTAC (protein) (Figures 2B, 2C, and S2). Notably, Nestin exhibited a consistently high positive correlation coefficient with CD97 in both mRNA (Figure 2B) and protein (Figure 2C) levels of all public databases ($R > 0.2$). While CD44, CD15, and CD49f showed positive correlations in all databases, the R-values for these correlations were not consistently high across the databases (some were below 0.1) (Figure S2).

To provide more direct evidence of the positive correlation between CD97 and GSC markers, we compared CD97 expression with aforementioned GSC markers by flow cytometry analysis (Figure 2D). We found that almost all intracellular GSC markers, such as Nestin, Oct3/4, and Nanog, showed high co-staining with CD97 in 83 and X01 cells ranging from 75.6% to 98.7%, and GSC772 cells with moderate CD97 expression showed over half co-staining (Figure 2D). However, some of the intracellular markers, in contrast to CD97, also showed overexpression in the general GBM cell line (U87 and U251; Figure S3). In addition, 83 and X01 cells did not contain any cells

CellPress
OPEN ACCESS

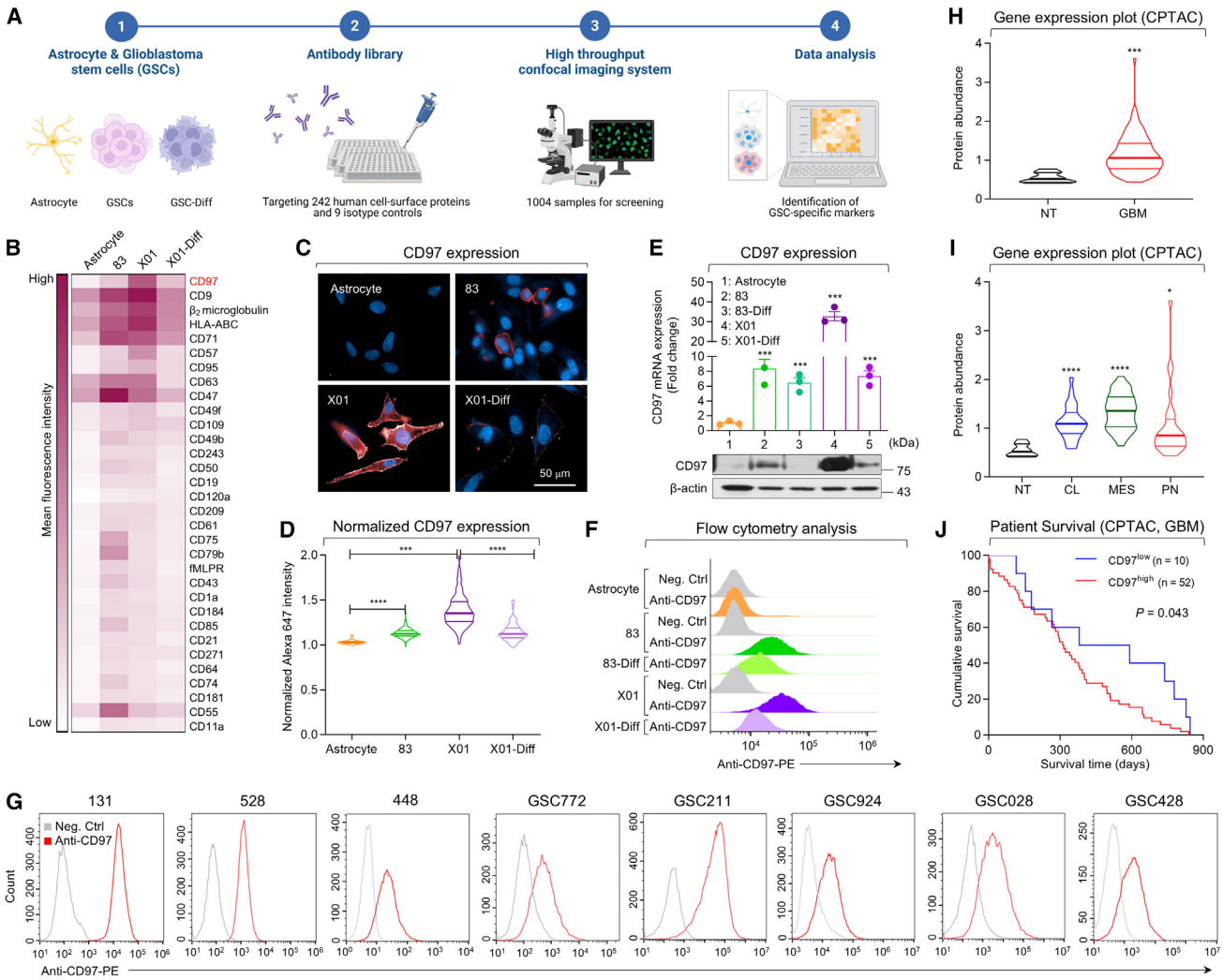

Figure 1. Identification of surface antigens for GSCs

(A) Schematic illustrating the experimental design. Human astrocytes and GSCs (83 and X01) were profiled using multiple antibody libraries.

(B) Heatmap showing the top 32 genes of human cell surface antigens, ranked based on the fold change values of fluorescence intensity compared to normal astrocytes or differentiated GSCs.

(C and D) High-throughput confocal immunofluorescence (IF) staining images showing staining with the anti-CD97 antibody (C) and quantification of fluorescence in the antibody array (values normalized to those of astrocytes) (D). Scale bar, 50 μm. All error bars represent the mean ± standard error of the mean (SEM; $n = 3$ independent experiments).

(E) Quantitative reverse-transcription PCR (RT-qPCR) and immunoblot (IB) analyses of CD97 expression in astrocytes, GSCs, and serum-differentiated GSCs (83-Diff and X01-Diff). β-actin was used as a loading control. Error bars represent the mean ± standard deviation (SD; $n = 3$ independent experiments).

(F) Flow cytometry analysis of astrocytes, GSCs, and serum-differentiated GSCs (83-Diff and X01-Diff) using a phycoerythrin (PE)-conjugated anti-CD97 antibody.

(G) Flow cytometry analysis of CD97 expression on patient-derived GSCs, stained with a PE-conjugated anti-CD97 antibody.

(H and I) CD97 protein expression in NT and GBM tissues (H) and the expression in each GBM subtype (I) according to the CPTAC database. NT, nontumor; CL, classical; MES, mesenchymal; NL, neural; PN, proneural.

(J) Kaplan-Meier overall survival curves for patients with GBM presenting high and low CD97 protein expression according to the CPTAC database. Groups were divided by optimal cutpoints using "survminer" R package.

The p value was determined using the log rank (Mantel-Cox) test. $^{****}p < 0.0001$, $^{***}p < 0.001$, $^{*}p < 0.05$, t test in (C), (D), (E), and (H). See also Figure S1.

with detectable CD133 expression, consistent with the findings from other reports.[46] CD44, another putative GSC surface marker, was detected with high expression in 83 cells (Figure 2D), as well as in a general glioma cell line, U87 (Figure S3A). Thus, CD44 is disqualified as a specific surface antigen for GSCs. Another GSC-specific surface antigen CD49f was detected in all GSCs (Figures 2D and S3), but did not exhibit a high positive correlation coefficient with CD97 expression in public databases (Figure S2). CD15 has also been reported as a GSC-enriched surface marker, but it showed no detectable

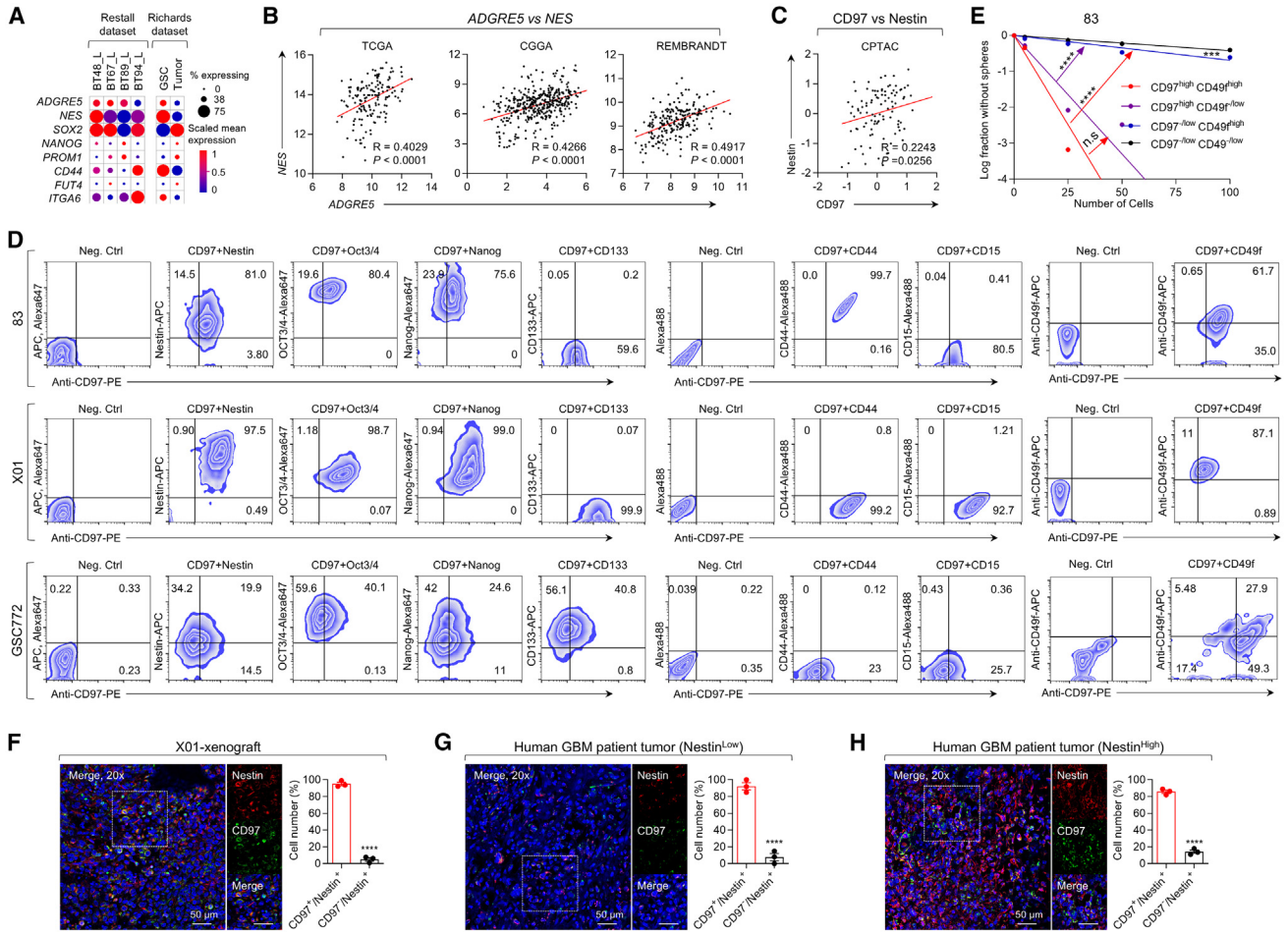

Figure 2. Validation of CD97 as an optimal GSC marker

(A) Bubble plot comparing expression of ADGRE5/CD97 and stem cell-related genes on GSCs and GBM tumors using single-cell RNA sequencing datasets from the study by Restall and Richards.

(B) Scatterplots to compare the RNA expression level of *ADGRE5* and *NES* according to patients with GBM in the TCGA, CCGA, and REMBRANDT databases. CD97 is encoded by *ADGRE5* gene. Nestin is encoded by *NES* gene.

(C) Scatterplots to compare the protein expression level of CD97 and Nestin according to patients with GBM in the CPTAC database.

(D) Flow cytometry plots in which CD97-PE was co-stained along with other GSC markers, including Nestin, Oct 3/4, Nanog, CD133 or CD49f, CD15, or CD44 in 83, X01, and GSC772. Each gate on the x and y axis separates positive from negative cells. The numbers in each quadrant indicate the percentages of cells.

(E) Limiting dilution assay (LDA) using $CD97^{high}$ $CD49f^{high}$, $CD97^{high}$ $CD49f^{-/low}$, $CD97^{-/low}$ $CD49f^{high}$, and $CD97^{-/low}$ $CD49f^{-/low}$ GSC 83 cells sorted through flow cytometry.

(F–H) Confocal images of CD97 (green) and Nestin (red) co-immunofluorescence staining in brain tissues of the X01-xenograft (F) and human patients with GBM who have $Nestin^{Low}$ (G) and $Nestin^{High}$ (H). Scale bar, 50 μm. Quantification analysis of the percentage of the cell number $CD97^+/Nestin^+$ and $CD97^-/Nestin^+$ cells. All error bars represent mean ± SD (n = 3 independent experiments) in (E)–(H). ****$p < 0.0001$, ***$p < 0.001$, t test. n.s, non-significant. See also Figures S2–S5.

expression in our tested GSCs (Figure 2D). Moreover, the immunoblotting analysis showed that CD97 expression was associated with a downregulation of typical intracellular marker expression under serum-induced differentiation conditions of GSCs (Figure S4). To further confirm the self-renewal ability of $CD97^+$ GSCs compared with other GSC makers, we performed flow cytometry to categorize GSCs (83, X01, and 528) into four distinct groups with CD49f: $CD97^{high}$ $CD49f^{high}$, $CD97^{high}$ $CD49f^{-/low}$, $CD97^{-/low}$ $CD49f^{high}$, and $CD97^{-/low}$ $CD49f^{-/low}$. We then evaluated the self-renewal capacity of these GSCs through limiting dilution assay (LDA). Supportively, the results demonstrated a gradient decrease in sphere formation abilities across these groups, with $CD97^{high}$ $CD49f^{high}$, $CD97^{high}$ $CD49f^{-/low}$, $CD97^{-/low}$ $CD49f^{high}$, and $CD97^{-/low}$ $CD49f^{-/low}$. This indicates that CD97 expression is significantly positively correlated with sphere formation ability in GSCs (Figures 2E and S5). Taken together, unlike intracellular markers that can unambiguously identify GSCs, currently used surface antigens, except for CD97, do not clearly define a comprehensive GSC population.

To further validate CD97 as a GSC-specific surface antigen, we conducted IF staining using X01 GSC xenograft GBM tissues

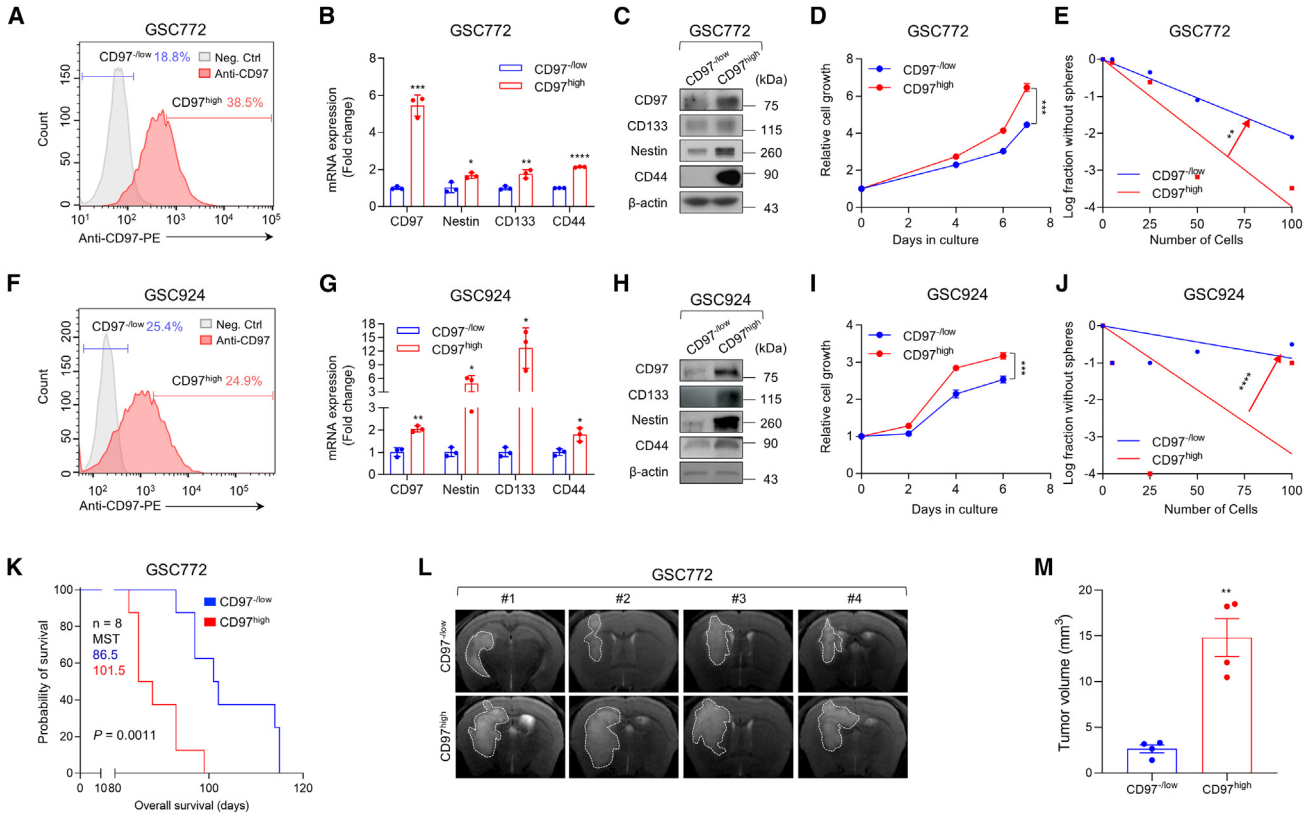

Figure 3. Characterization of CD97^{high} cells *in vitro* and *in vivo*

(A) GSC772 cells were stained with an anti-CD97 antibody and analyzed using flow cytometry. The Neg.Ctrl group is shown in gray and the Anti-CD97 group is shown in red.

(B–E) RT-qPCR (B) and IB analysis (C) of stemness-related genes, proliferation assays (D), and LDAs (E) in the CD97^{high} and CD97$^{-/low}$ subpopulations of GSC772. β-actin was used as a loading control.

(F) GSC924 cells were stained with an anti-CD97 antibody and analyzed using flow cytometry as in (A).

(G–J) RT-qPCR (G) and IB analysis (H) of stemness-related genes, proliferation assays (I), and LDAs (J) in the CD97^{high} and CD97$^{-/low}$ subpopulations of GSC924. GAPDH was used as a loading control.

(K) Kaplan-Meier survival curves of mice orthotopically implanted with CD97^{high} or CD97$^{-/low}$ GSC772 cells (n = 8, 2.5 × 10^5 cells/mouse). MST, median survival time. Log rank (Mantel-Cox) test.

(L and M) Representative axial MRI (L) and the quantified tumor size (M) of mice bearing orthotopic xenografts of CD97^{high} or CD97$^{-/low}$ GSC772 cells. Regions of interest (ROIs) within the tumor are indicated by white polygons.

All error bars represent mean ± SD (n = 3 independent experiments). ****p < 0.0001, ***p < 0.001, **p < 0.01, *p < 0.05, t test in (B)–(J), (L), and (M).

(Figure 2F). The results showed that most of the Nestin-positive cells, known as GSCs, were co-stained with CD97, supporting the highly positive correlation between Nestin and CD97. In addition, the Nestin-positive GBM cells showed high co-localization with CD97 in Nestin^{Low} and Nestin^{High} patient GBM tissues (Figures 2G and 2H), further supporting that CD97 is an optimal GSC surface marker. These findings collectively support the potential utility of CD97 as a surface antigen for GSCs.

To verify CD97 as a GSC surface antigen and its function in GBM initiation, we examined the characteristics of CD97-enriched GSCs. GSC772 was grouped into two subpopulations based on CD97 expression profiles; the top 38.5% was defined as CD97^{high}, and the bottom 18.8% was defined as CD97$^{-/low}$ using flow cytometry (Figure 3A). The isolated CD97^{high} population exhibited high expression of the stemness-related markers CD133, Nestin, and CD44 at both the mRNA and protein levels compared to the CD97$^{-/low}$ population (Figures 3B and 3C). As expected, sorted CD97^{high} cells showed significantly increased proliferation (Figure 3D) and self-renewal (Figure 3E) compared to CD97$^{-/low}$ cells. Additionally, we replicated these findings by sorting GSC924 based on CD97 expression and confirming the enrichment of stem cell markers and the promotion of cell growth and self-renewal in CD97^{high} cells (Figures 3F–3J).

Next, to identify the *in vivo* tumorigenic potential of CD97-enriched GSCs, we established orthotopic transplantation models using CD97^{high} and CD97$^{-/low}$ GSC772. The overall survival of tumor-bearing animals was significantly shorter in the CD97^{high} GSC772-injected group (86.5 days) than in the CD97$^{-/low}$ GSC772-injected group (101.5 days) (Figure 3K). Importantly, the onset of tumors was significantly faster, and magnetic resonance imaging (MRI) at 70 days after implantation showed that the tumors derived from CD97^{high} GSC772 were significantly

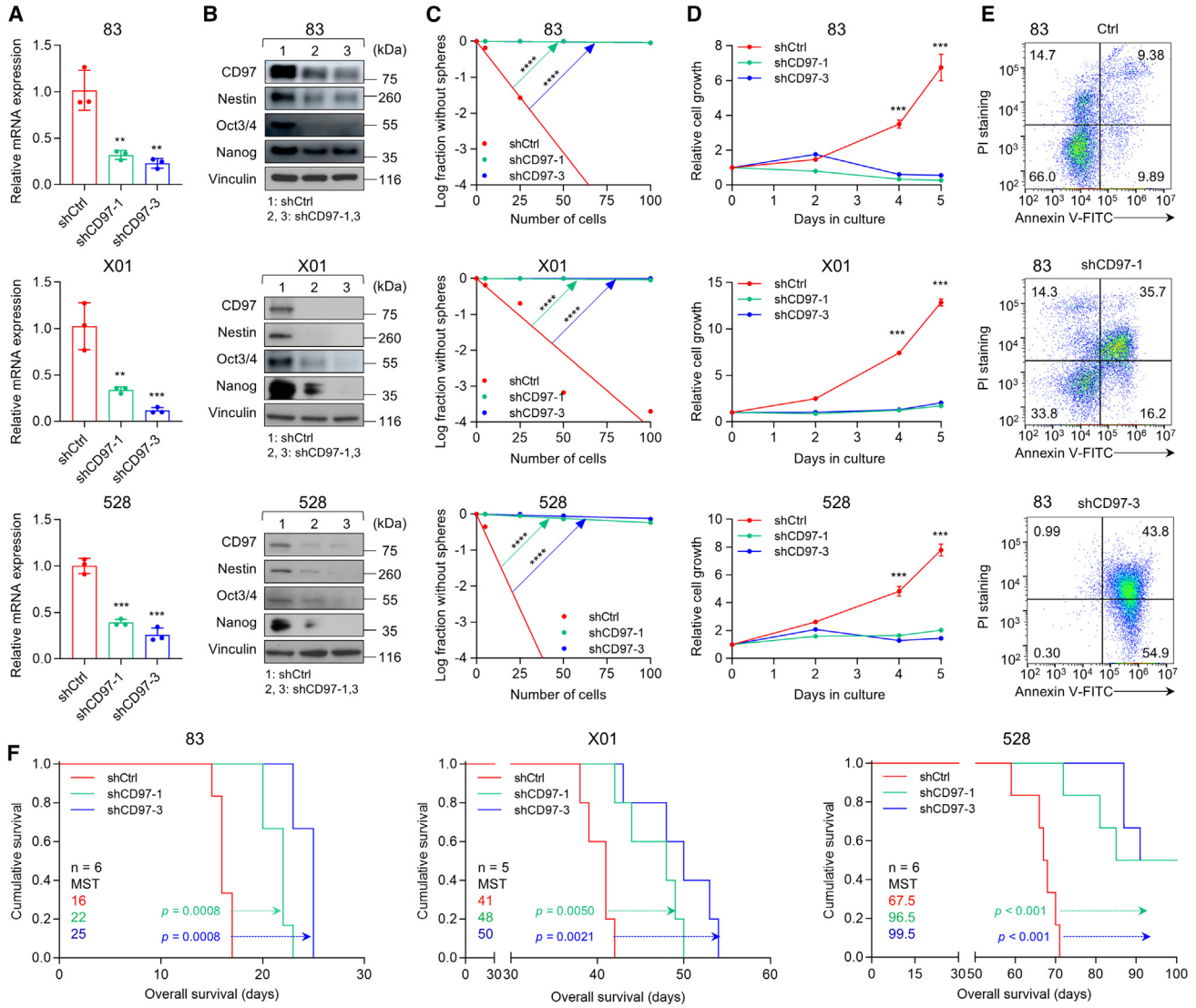

Figure 4. CD97 regulates GSC tumorigenicity

(A–D) RT-qPCR (A) of CD97 expression, IB analysis (B) of GSC intracellular markers, LDAs (C), and cell proliferation assays (D) in three different GSCs (83, X01, and 528 cells) infected with shCtrl, shCD97-1, or shCD97-3 lentivirus. β-actin, GAPDH, and vinculin were used as loading controls. All error bars represent mean ± SD (n = 3 independent experiments). ****p < 0.0001, ***p < 0.001, **p < 0.01, t test.

(E) Flow cytometry analysis of Annexin V and PI staining in GSCs 83 infected with shCtrl, shCD97-1, or shCD97-3 lentivirus.

(F) Kaplan-Meier survival curves of mice bearing orthotopic xenografts of three GSCs infected with shRNA lentivirus (n = 5 or 6, 1 × 10^4 for 83 and X01, or 1 × 10^5 for 528 cells/mouse). MST, median survival time. Log rank (Mantel-Cox) test.

See also Figures S6–S10.

larger than those derived from CD97$^{-/low}$ GSC772 (Figures 3L and 3M). Overall, these data strongly indicate that CD97^{high} cells have the characteristics of GSCs *in vitro* and high tumorigenicity *in vivo*.

The presence of GSCs implies the ability to proliferate indefinitely and exhibits a high degree of plasticity, contributing to the intratumor heterogeneity observed in GBM.[47] To explore the role of CD97 in maintaining GSC tumorigenicity, we manipulated CD97 expression in three types of GSCs (83, X01, and 528) with the highest CD97 expression among all tested GSCs, performed an *in vitro* LDA and proliferation assay, and generated an orthotopic mouse model. Silencing CD97 with two independent short hairpin RNA (shRNA)-expressing lentiviruses significantly reduced CD97 mRNA and protein expression (Figures 4A and 4B). Additionally, CD97 knockdown in GSCs resulted in the downregulation of intracellular GSC markers (Nestin, Oct3/4, and Nanog), as confirmed by immunoblotting (Figure 4B) and flow cytometry analysis (Figure S6). Consequently, CD97 knockdown significantly led to decreased sphere-forming ability of GSCs, as measured using LDA, a

renowned method to determine the GSC self-renewal capacity (Figure 4C). CD97 knockdown significantly decreased GSC proliferation and increased cell death (Figures 4D, 4E, and S7). CD97 knockout further confirmed the downregulation of GSC markers, along with reduced sphere-forming ability and cell growth in GSCs (Figure S8). However, CD97 knockdown in $CD97^{-/low}$ GSCs and non-GSCs did not show much effect on cell growth or expression of stemness markers (Figure S9). Furthermore, we observed the restoration of self-renewal capacity and cell proliferation, underscoring the role of CD97 in these processes, in rescue experiments where CD97 was re-expressed in the CD97-knockdown cells (Figure S10). Then, we investigated the role of CD97 in the tumor progression of GBM by intracranially injecting mice with GSCs transduced with shCtrl or shCD97s. Knockdown of CD97 expression in 83, X01, and 528 GSCs remarkably prolonged the survival of the mice (Figure 4F). Collectively, these results highlight that CD97 expression is crucial for maintaining GSC tumorigenicity processes, including self-renewal, proliferation, and tumor progression.

Screening downstream targets of CD97 in GSCs

We used an integrated approach to comprehensively determine the biological functions mediated by CD97 expression and to understand the regulatory role of CD97. We performed transcriptome profiling using RNA sequencing (RNA-seq) analysis with 83, X01, and 528 GSCs after the knockdown of CD97 and found that 131 genes were significantly downregulated by silencing CD97 in all of those GSCs (Figure 5A). Gene Ontology Biological Process analysis showed enrichment in the regulation of stem cell population maintenance in the shCtrl group, indicating a potential role of CD97 in GSC maintenance (Figure 5B). Each gene identified as being downregulated upon CD97 knockdown was carefully examined for its significant functions in biological processes. Thus, the biological process category of Gene Ontology terms was analyzed for enrichment of these commonly downregulated genes using the Database for Annotation, Visualization, and Integrated Discovery. The results showed that cell-cell adhesion, nucleobase-containing compound metabolic processes, and positive regulation of hormone biosynthetic processes were the only three significantly enriched signaling pathways in GSCs with CD97 knockdown (Figure 5C). Among them, cell-cell adhesion showed the highest gene ratio, which included poly(rC)-binding protein 1 (*PCBP1*), basigin (*BSG*), Rho GTPase-activating protein 1 (*ARHGAP1*), basic leucine zipper and W2 domain-containing protein 1 (*BZW1*), basic leucine zipper and W2 domain-containing protein 2 (*BZW2*), and drebrin (*DBN1*) (Figure 5C). Indeed, the downregulation of the mRNA expression of these cell-cell adhesion-associated genes was confirmed in GSCs with CD97 knockdown (Figure 5D). To determine the possible relationship between the expression of CD97 and these related genes, we analyzed the clinical prognosis using publicly available GBM datasets and found that patients expressing high levels of both CD97 and ARHGAP1, BZW1, or BZW2 experienced worse survival outcomes than patients with low levels in TCGA (Figure 5E), CGGA (Figure S11A), and REMBRANDT databases (Figure S11B), while coexpression of CD97 and BSG, DBN1, or PCBP1 did not consistently show significant correlations with the survival probability of patients in either database (Figures S11C–S11E). Furthermore, we assessed the regulators of the cell-cell adhesion-associated genes by analyzing the 50 hallmark signaling pathways along with the transcriptome results using gene set enrichment analysis. Among the significant hallmark signaling pathways enriched in the shCtrl group, we observed that mTOR signaling pathways (including PI3K/AKT/mTOR, also known as mTORC1 and mTORC2) were enriched in the shCtrl group (Figures 5F and 5G). Therefore, we hypothesize that among the candidate genes, CD97 regulates the expression of *ARHGAP1*, *BZW1*, and *BZW2* through mTOR signaling.

CD97 regulates downstream gene expression through mTORC2 signaling

mTOR is an intracellular serine/threonine conserved protein kinase in two distinct complexes, mTORC1 and mTORC2. mTORC1, which is rapamycin sensitive, controls cell growth at least partially through its ability to phosphorylate S6K and activates downstream PI3K/AKT signaling.[48,49] On the other hand, by phosphorylating AKT on Ser473, mTORC2, which is rapamycin insensitive, regulates cell proliferation, survival, migration, and cytoskeletal remodeling.[50–52] As an extension of the aforementioned results, we rigorously tested the functions of the downstream signaling pathway for CD97. The isolated $CD97^{high}$ population regulated AKT phosphorylation (S473) related to mTORC2 signaling and exhibited increased expression of ARHGAP1, BZW1, and BZW2 (Figure S12A). Supportively, distinct staining with anti-ARHGAP1, anti-BZW1, and anti-BZW2 antibodies was detected in $CD97^{high}$ GSC772 tumors (Figure S12B). Additionally, silencing CD97 using shRNAs substantially attenuated S6K (S371 and T389) and AKT (T308 and S473) phosphorylation in three different GSCs (Figure 6A). Accordingly, the expression levels of ARHGAP1, BZW1, and BZW2 were significantly reduced in CD97-knockdown GSCs (Figure 6A). Next, we conducted rescue experiments with the three genes, *BZW1*, *BZW2*, and *ARHGAP1*, in CD97-knockdown GSCs. All of three genes overexpressed in CD97-knockdown GSCs partially rescued shCD97-mediated repression of GSC cell growth and self-renewal in three different GSCs (Figures 6B and S13). These results show that these three genes, associated with cell-cell adhesion, are key molecules in CD97-mediated mTOR signaling for the maintenance of GSC proliferation and self-renewal and prompted us to investigate the potential involvement of mTOR downstream of CD97.

Given the potential involvement of mTOR downstream of CD97, we subsequently aimed to identify mTORC1 or mTORC2 signaling involved with *ARHGAP1*, *BZW1*, and *BZW2* gene expression by administering small-molecular inhibitors. Torin1 (an inhibitor of mTORC1 and mTORC2) and AKT inhibitor IV induced decreases in not only the phosphorylation of S6K (S371 and T389) and AKT (T308 and S473) but also the expression of three target molecules (Figures 6C and 6D). Subsequently, we blocked each signaling pathway with two different classes of mTOR-specific inhibitors (rapamycin, a mTORC1 inhibitor, and JR-AB2-011, a mTORC2 inhibitor) and analyzed the functional state of each pathway in GSCs to understand the

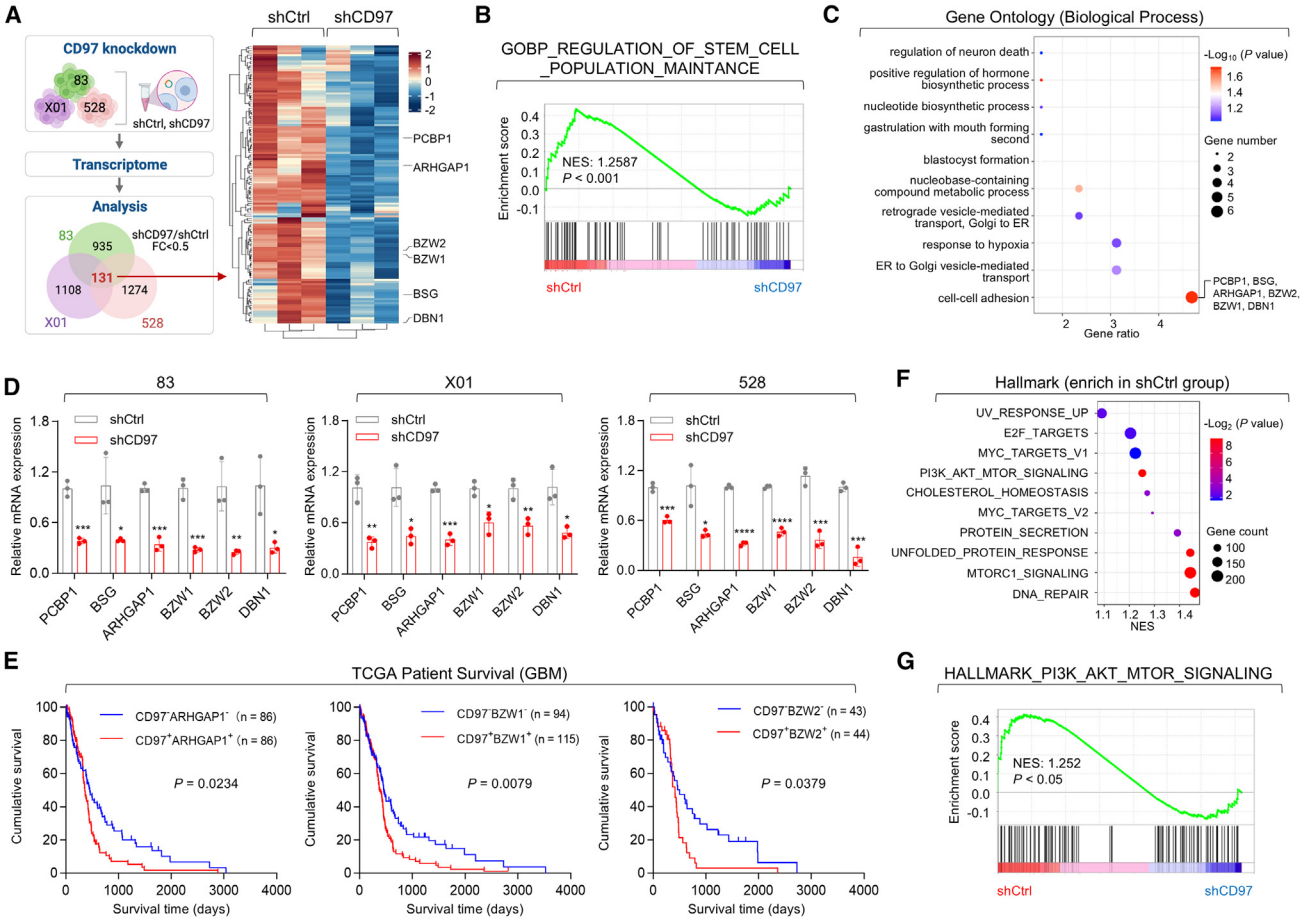

Figure 5. Screening of downstream targets of CD97 in GSCs

(A) Schematic representation of the experimental strategy for the transcriptome analysis. Heatmap of the hierarchical clustering analysis showing the expression of 131 common downregulated genes in CD97-knockdown GSCs (right).

(B) Gene set enrichment analysis (GSEA) plot for the regulation of stem cell population maintenance signature from the Gene Ontology Biological Process (GOBP) category comparing the shCtrl and shCD97 groups. NES, normalized enrichment score.

(C) Bubble chart showing the top 10 biological processes of Gene Ontology terms for genes downregulated in CD97-knockdown GSCs. Size, gene number; color, $-\log_{10}$ (p value).

(D) RT-qPCR of PCBP1, BSG, ARHGAP1, BZW1, BZW2, and DBN1 expression in three different GSCs (83, X01, and 528 cells) infected with shCtrl or shCD97 lentivirus. β-actin was used as a loading control. All error bars represent mean ± SD (n = 3 independent experiments). ****$p < 0.0001$, ***$p < 0.001$, **$p < 0.01$, *$p < 0.05$, t test.

(E) Kaplan-Meier overall survival curves for patients with GBM presenting the high and low expression of the CD97/ARHGAP1 (left), CD97/BZW1 (middle), and CD97/BZW2 (right) mRNAs according to TCGA GBM database. Log rank (Mantel-Cox) test.

(F) Bubble chart showing the top 10 hallmark genes enriched in shCtrl GSCs. Size, gene number; color, $-\log_2$ (p value).

(G) GSEA plot for the PI3K/AKT/mTOR signaling signature from the Hallmark category comparing the shCtrl and shCD97 groups.

See also Figure S11.

mechanism by which signaling triggered by CD97 contributes to the expression of its target genes. Rapamycin treatment reduced the phosphorylation of S6K (S371 and T389) but did not consistently alter the expression levels of the three target proteins (Figure 6E). On the other hand, treatment with JR-AB2-011 altered the phosphorylation of AKT (S473), which is important for mTORC2 activation, and, interestingly, downregulated the expression of three target proteins (Figure 6F). Based on the cell proliferation assay and LDA, all inhibitors that selectively inhibited mTOR/AKT signaling therapeutically blocked the growth and self-renewal of GSCs since our results suggested that CD97 activates mTORC1 and mTORC2 signaling, but only mTORC2 is involved in downstream gene expression (Figures 6G and S14). In animal models, JR-AB2-011 treatment significantly decreased tumor size and prolonged the survival of mice bearing X01-Luc (X01 GSC transduced with a luciferase-expressing vector) orthotopic xenograft tumors (Figures 6H and S15A); also, reduced mTOR2 involved downstream gene expression (Figure S15B). Collectively, these data strongly suggest that CD97 regulates ARHGAP1, BZW1, and BZW2 expression through the mTORC2/AKT pathway, which is involved in the tumorigenesis of GSCs (Figure 6I).

CellPress
OPEN ACCESS

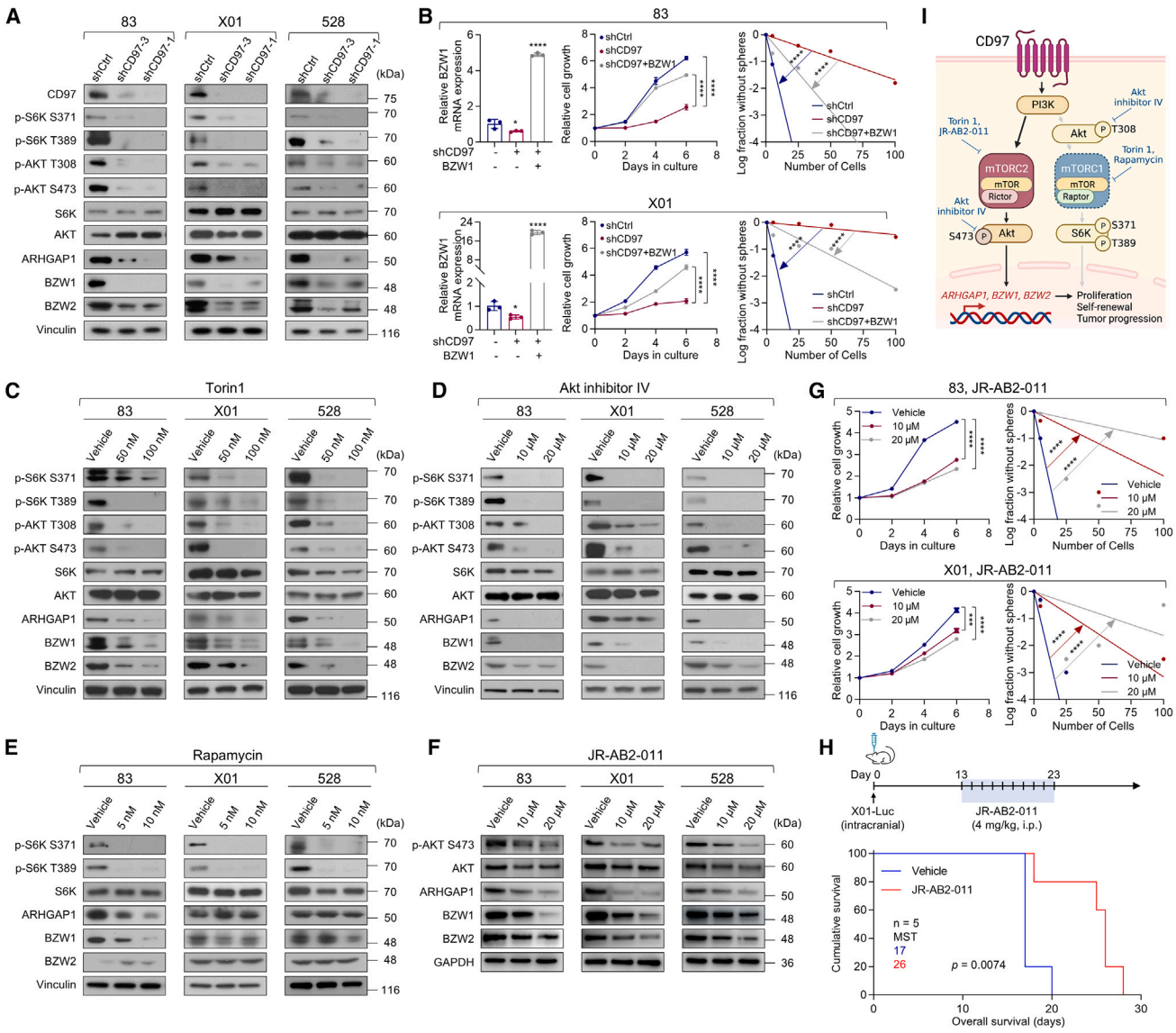

Figure 6. mTORC2 inhibition prevents proliferation and self-renewal in GSCs

(A) IB analysis of CD97, p-S6K, p-AKT, S6K, AKT, ARHGAP1, BZW1, and BZW2 levels in three different GSCs (83, X01, and 528 cells) infected with shCtrl or shCD97 lentivirus.

(B) RT-qPCR of BZW1 expression (left), cell proliferation assay (middle), and LDAs (right) in 83 and X01 GSCs infected with shCtrl and shCD97 lentivirus, followed by BZW1 lentivirus infection.

(C–F) IB analysis of p-S6K, p-AKT, S6K, AKT, ARHGAP1, BZW1, and BZW2 levels in three different GSCs (83, X01, and 528 cells) treated with Torin1 48 h (C), AKT inhibitor IV 24 h (D), 24 h rapamycin (E), and JR-AB2-011 24 h (F).

(G) Cell proliferation assays (left) and LDAs (right) were performed on 83 and X01 GSCs after treatment with JR-AB2-011.

(H) Kaplan-Meier survival curves of mice orthotopically implanted with X01-Luc cells (n = 5, 1 × 10^5 cells/mouse) and intraperitoneally (i.p.) treated with JR-AB2-011 (4 mg/kg) or vehicle. MST, median survival time. Log rank (Mantel-Cox) test.

(I) Schematic representation of the CD97-related signaling pathway regulating the proliferation, self-renewal, and tumor progression of GSCs. Vinculin and GAPDH, and β-actin were used as loading controls in IB, β-actin was used as a loading control in RT-PCR.

All error bars represent mean ± SD (n = 3 independent experiments) in (B) and (G). ****$p < 0.0001$, ***$p < 0.001$, *$p < 0.05$, t test. See also Figures S12–S15.

Development of CD97-targeting CAR Th9 cells and their antitumor activity

Cell surface antigens might be good targets for one of the most promising anticancer therapies, known as CAR T cells, which have developed artificial molecules capable of recognizing and subsequently destroying cancer cells that specifically express antigens on their surface.[53–55] The biologically relevant properties of the CD97 antigen suggest that it may be an attractive candidate therapeutic target for GBM CAR T cell therapy. In this study, our approach focuses on the development of

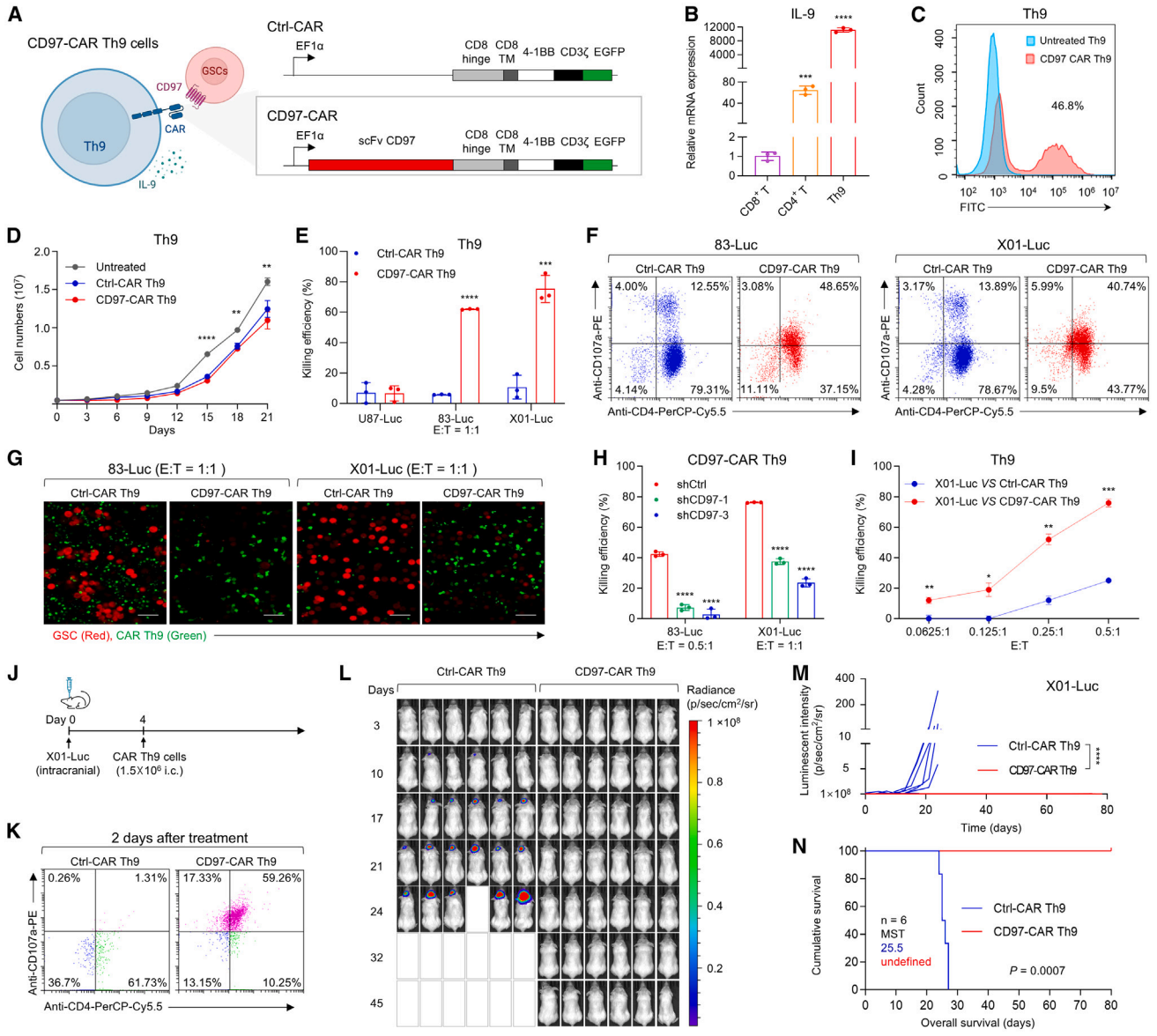

Figure 7. Antitumor activity of CD97-targeting CAR Th9 cells against GBM

(A) Schematic showing the structure of the second-generation lentiviral vectors encoding CD97-CAR, including the 4-1BB and CD3ζ costimulatory domains. TM, transmembrane domain.

(B) RT-qPCR analysis of IL-9 expression in $CD8^+$ T cells, $CD4^+$ T cells, and Th9 cells.

(C) Flow cytometry analysis of CAR expression detected by the fusion protein EGFP.

(D) Expansion kinetics of untreated, Ctrl-CAR, and CD97-CAR T cells *in vitro* (n = 3 independent experiments).

(E) Antigen-specific *in vitro* cytotoxicity of CD97-CAR Th9 cells or Ctrl-CAR Th9 cells toward U87-Luc, 83-Luc, or X01-Luc cells, evaluated using a luciferase activity assay.

(F) Flow cytometry analysis of CD4 and CD107a expression on CD97-CAR Th9 cells following incubation with 83-Luc and X01-Luc cells.

(G) Representative confocal microscopy images showing CD97-CAR Th9 cells or Ctrl-CAR Th9 cells interacting with 83-Luc and X01-Luc cells at an E:T ratio of 1:1 for 24 h. Scale bar, 50 μm.

(H and I) Antigen-specific *in vitro* cytotoxicity of CD97-CAR Th9 cells toward 83-Luc or X01-Luc cells infected with shCD97 or shCtrl lentivirus (H) and against X01-Luc cells at different E:T ratios (I).

(J) Schematic experimental design to evaluate the antitumor effects of CD97-targeting CAR Th9 cells. Mice were implanted with X01-Luc cells (n = 6, 1 × 10^5 cells/mouse) and intracranially injected with CD97-CAR or Ctrl-CAR Th9 cells (1.5 × 10^6 cells/mouse) on day 4.

(K) Flow cytometry analysis showing the expression of CD4 and CD107a within the tumor two days post-treatment of CD97-CAR Th9 or Ctrl-CAR Th9 cells.

(L) Bioluminescence images of mice as in (J).

(legend continued on next page)

CD97-targeting CAR Th9 cells, a subset of CD4$^+$ T cells characterized by their production of interleukin 9 (IL-9).[56,57] Recent studies have indicated that Th9 cells possess the capability to exert potent cytolytic activity against tumor cells, exhibit reduced exhaustion, and maintain long-term persistence.[56,58] First, we generated an anti-CD97 human antibody in a hybridoma and characterized the extracellular single-chain variable fragment (scFv) sequence of CD97 (Figure S16A). Next, we designed and created a second-generation lentiviral CD97-CAR construct with the aforementioned validated CD97-specific scFv fused with intracellular signaling domains, including 4-1BB and CD3ζ (Figure 7A). The CD97-CAR lacking the scFv sequences was used as a control (control CAR, Ctrl-CAR). Then, CD97-CAR was successfully transduced into Th9 cells with high IL-9 expression (Figure 7B) through the transduction efficiency detected by the GFP signal using flow cytometry and representative fluorescence imaging analyses (Figures 7C and S16B), and the CD97-CAR Th9 cells sustained expansion for 3 weeks (Figure 7D). The CD97-CAR Th9 cells exhibited significantly greater expansion capacity and cytotoxic activity compared to both CD97-CAR peripheral blood mononuclear cell and CD97-CAR CD8$^+$ T cells (Figures S16C and S16D). Following transduction and expansion, we co-cultured CD97-CAR Th9 cells or Ctrl-CAR Th9 cells with GSCs (83-Luc and X01-Luc cells) and non-GSC U87-Luc cells at an effector-to-target (E:T) ratios of 1:1 to assess the functionality of CD97-CAR Th9 cells *in vitro*. CD97-CAR Th9 cells demonstrated robust cytotoxic activity against 83-Luc and X01-Luc GSCs, both of which exhibit high levels of CD97 expression (Figure 7E). Additionally, CD97-CAR Th9 cells or Ctrl-CAR Th9 cells were co-cultured with 83-Luc GSC at 2:1 and 5:1 E:T ratios to further evaluate the specific tumor-killing ability of CD97-CAR Th9 cells (Figure S17A). Since CD107a, a marker for degranulation of cytotoxic lymphocytes, is utilized to investigate CAR T cell activation and its triggering of cytotoxic effects,[59] we examined surface CD107a expression on CAR Th9 cells co-cultured with GSCs via multi-parameter flow cytometry. The percentages of CD4$^+$ CD107a$^+$ T cells were increased to more than 40% in CD97-CAR Th9 cells compared to Ctrl-CAR Th9 cells with around 13%, demonstrating cytotoxicity and the degranulation capacity *in vitro* (Figure 7F). To further confirm the cytotoxicity and degranulation capacity of CD97-CAR Th9 cells, we assessed the expression of IFN-γ, a key marker of cytotoxic lymphocyte degranulation. The percentage of CD4$^+$ IFN-γ$^+$ Th9 cells was higher in CD97-CAR Th9 cells compared to Ctrl-CAR Th9 cells when cultured with 83-Luc and X01-Luc GSCs (Figure S17C). Moreover, when CD97-CAR Th9 cells or Ctrl-CAR Th9 cells were co-cultured with RFP lentivirus-transfected GSCs (83-Luc and X01-Luc GSCs) at an E:T ratios of 1:1 for 24 h, subsequent confocal analysis revealed that CD97-CAR Th9 cells exhibited a stronger tumor-killing ability compared to Ctrl-CAR Th9 cells (Figures 7G and S17B). Furthermore, the co-culture of 83-Luc and X01-Luc cells with CD97 knockdown mediated by shRNAs with CD97-CAR Th9 cells decreased CAR Th9 cell cytotoxic efficacy (Figure 7H). We further analyzed the CD97-CAR Th9 cytotoxic effect at different lower co-culture E:T ratios (0.0625:1, 0.125:1, 0.25:1, and 0.5:1); X01-Luc cells were selected as a high performer in terms of CD97-CAR antitumor activity (Figure 7I). Together, these data reveal robust, antigen-specific CD97-CAR Th9 cell responses upon contact with CD97$^+$ GSCs.

To further validate the CD97-targeting therapeutic strategy, we first assessed the efficacy of *in vivo* tumor-killing activity of CD97-CAR Th9 cells by intravenous injections using an orthotopic model of X01-Luc cells (Figures S17D–S17H). Compared to mice treated with untreated T cells, CD97-CAR T cells significantly increased the CD4$^+$ CD107a$^+$ T cell population at 2 and 7 days after injection, reduced tumor growth, reversed body weight loss, and improved the survival rate of the mice (Figures S17E–S17H). These findings highlight the potent *in vivo* tumor-killing efficacy of CD97-targeting therapy. Given the clinical studies have demonstrated that locally targeted CAR T cell therapy for GBM, when administered directly into the brain, effectively overcomes inter- and intra-patient heterogeneity and circumvents the blood-brain barrier, this method has proven to be safe and clinically effective in select patients.[60,61] In light of these findings, we next investigated the *in vivo* tumor-killing activity of CD97-CAR Th9 cells through intracranial injections to further validate the efficacy of the CD97-targeting CAR Th9 cell therapeutic strategy. Mice orthotopically injected with X01-Luc were given intracranial injections with 1.5 × 10^6 CD97-CAR Th9 cells or Ctrl-CAR Th9 cells on day 4 (Figure 7J). We first examined surface CD107a expression on CD97-CAR Th9 cells in the tumor. The percentage of CD4$^+$ CD107a$^+$ T cells was increased to 59.26% after 2 days of intracranial injections of CD97-CAR Th9 cells (compared with 1.31% in Ctrl-CAR Th9 cell-injected group, Figure 7K) and remained at 48.36% until 7 days (Figure S17I), demonstrating cytotoxicity and the degranulation capacity *in vivo*. Continuing with the investigation, the CD97-CAR Th9 cells remarkably reduced tumor growth without losing body weight, as evidenced by bioluminescence measurements (Figures 7L, 7M, and S17J). Moreover, the CD97-CAR Th9 cells led to a substantial and significantly improved survival rate compared to that achieved with Ctrl-CAR Th9 cells (Figure 7N). To further validate the antitumor efficacy and potential toxicity of CD97-CAR T cells, we developed a murine version of the CD97 CAR. This version utilizes the same human CD97 scFv while substituting the human signaling molecules with murine CD28 and CD3ζ (mCD97-CAR), in accordance with the methodologies described in the referenced literature.[62,63] Activated murine T cells were subsequently transduced with this vector to enable CAR expression. Although the transfection efficiency was only 11% (Figure S18A), the cytotoxic killing ability of mCD97-CAR T cells

(M) Quantification of bioluminescence intensity of photons emitted from each tumor in the images in (L). Data are presented as mean ± SD, two-way ANOVA at day 24, ****$p < 0.0001$.

(N) Kaplan-Meier survival curve of mice as in (J). MST, median survival time. Log rank (Mantel-Cox) test. GAPDH was used as a loading control.

All error bars represent mean ± SD ($n = 3$ independent experiments) in (B), (D), (E), (H), and (I). ****$p < 0.0001$, ***$p < 0.001$, **$p < 0.01$, *$p < 0.05$, t test. See also Figures S16–S18.

increased gradually as the E:T ratios in the co-culture with CD97-overexpressing murine syngeneic GBM cells (GL261-Luc-CD97) were raised (1:1, 5:1, and 10:1) (Figures S18A and S18B). Next, mice orthotopically injected with GL261-Luc-CD97 received intracranial injections with 1 × 10^6 mCD97-CAR T cells or untreated T cells on day 4 (Figure S18C). The results showed that treatment with mCD97-CAR T cells significantly reduced tumor growth, reversed body weight loss, and markedly improved the survival rate of mice compared to those treated with untreated T cells (Figures S18C–S18F). Collectively, our results highlight that CD97-specific targeting of CAR Th9 cells exerts potent antitumor effects on the GBM xenograft model and potentially represents a new therapeutic option for GBM.

DISCUSSION

In the current study, we identified CD97 as an optimal GSC-enriched antigen that promotes GSC tumorigenicity via the mTORC2/AKT signaling axis, which increases *ARHGAP1*, *BZW1*, and *BZW2* gene expression. Moreover, we developed CD97-targeting CAR Th9 cells that exerted a potent cytolytic effect and significantly prolonged the survival rate of a mouse xenograft model. Given the dire prognosis of GBM and the absence of effective therapies to treat GBM, CD97-CAR Th9 cell therapy may represent a promising option for patients with GBM.

GSC identification has been dependent on intracellular neural stem cell-associated proteins[64] or the utilization of diverse surface antigens, employing combinations of double or multidimensional expression with varying levels of effectiveness.[11–21] Intracellular markers of the GSC, including Nestin, Oct3/4, and Nanog, show high expression in neurosphere cultures and are required for the maintenance of GSC identity.[42,64] However, intracellular neural stem cell-associated proteins were also expressed in non-GSC cells, suggesting that GSC-specific expression of these intracellular markers is not necessarily defined as GSC markers.[65,66] We also analyzed the expression levels of the representative GSC surface antigens, including CD133, CD44, CD15, and CD49f. Here, our results revealed that CD133 is high (GSC772 cells, over 90%) or rarely expressed (83 and X01 cells, less than 1%) in GSCs, and also expressed in GBM cell lines (19%–24%). While CD44 is a mesenchymal-like GSC antigen with high specificity (83 cells, 99.7%), CD44 also has strong positivity in U87 cell lines (100%), making it difficult to categorize as a GSC surface antigen. The CD15-positive population was rare and represented less than 5.5% of our tested GSCs and GBM cell lines. Another stemness marker, CD49f, closely aligns with CD97. The population of $CD97^{high}$ $CD49f^{high}$ and $CD97^{high}$ $CD49f^{-/low}$ GSCs significantly induced the sphere formation ability compared to $CD97^{-/low}$ $CD49f^{high}$ and $CD97^{-/low}$ $CD49f^{-/low}$ GSCs. Notably, $CD97^{high}$ $CD49f^{high}$ GSCs exhibited greater self-renewal capacity than both $CD97^{high}$ $CD49f^{-/low}$ and $CD97^{-/low}$ $CD49f^{high}$ GSCs, suggesting that CD97 could be a more reliable stemness marker for GSCs than CD49f. Moreover, CD97 is expressed in 23%–100% of the GSCs we analyzed, and GBM cell lines U87 and U251 show almost no or lower expression. Overall, our study highlights the limitations of using conventional surface antigens in identifying GSCs and emphasizes the potential utility of CD97 as an enriched surface antigen in GSCs.

While abundant CD97 expression has been reported in GBM, including those associated with GSC,[17,30,33,34,36,37] it remains largely unverified and limited mainly to *in vitro* studies.[28–37] The GSCs they used have some limitations: CD133-positive glioma-initiating cells in screening procedure[30] or adherent brain tumor-initiating cells for validation.[33] Additionally, recent studies have demonstrated the different mechanisms of CD97 involved in gliomagenesis. One study has demonstrated that the interaction of CD97 and β-arrestin promoted glycolytic metabolism by the mitogen-activated protein kinase pathway and developed an anti-CD97 antibody-drug conjugate that exhibited only an *in vitro* killing effect[36]; this group advocated CD97 as a regulator of tumor metabolism in GBM. Although the role of two functional CD97 fragments in GBM proliferation and invasion via $G\alpha_{12/13}$-mediated signaling, such as Rho pathway, are considered, the details remain unclear.[37] In the current study, we discovered the CD97 mechanism in the maintenance and tumorigenesis of GSCs, offering an entirely different perspective. Our comparative transcriptome analysis also reveals that CD97 controlled GSCs features by activating mTORC2-AKT (S473) signaling. Another recent study showed that upregulated CD97 in GBM promotes GBM cell invasion through PI3-AKT signaling,[35] but they validated using only a single type of GBM cell line (U251) *in vitro* and specifically the phosphorylated site (T308) implicated in mTORC1. Indeed, CD97 participates in both mTORC1 and mTORC2 signaling pathways, but cell-cell adhesion-related genes, such as *ARHGAP1*, *BZW1*, and *BZW2*, are regulated through the mTORC2 signaling pathway. The mTORC2 phosphorylates AGC kinases such as AKT, SGK, and PKC family members, each with known oncogenic roles in tumor cell survival[50–52] and metastasis.[66] Additionally, our findings suggest that downstream mTORC2-AKT signaling is involved in the maintenance of GSCs. Pharmacological inhibition of mTORC2 signaling with JR-AB2-011 significantly decreased GSC proliferation and self-renewal capacity and improved *in vivo* survival rate. Although our preclinical findings supported an important role in the CD97-dependent mTORC2 signaling pathway, it is still necessary to comprehensively analyze the safety profile of this inhibitor.

$CD4^+$ Th9 cells appear to function in a broad range of autoimmune disorders, allergic inflammation, and cancer and have recently been in the spotlight.[57,67] Several investigations have identified that $CD4^+$ T cells also have direct antitumor activity, even though their role is broadly presumed to be as helper cells providing proinflammatory cytokines and chemokines.[57,58,68–70] $CD4^+$ T cells directly interacted with microglia, promoting IFN-γ-dependent microglia activation and phagocytosis in GBM,[69] and orchestrated with tumor-associated myeloid cells, triggering remote inflammatory cell death that indirectly eradicates IFN-unresponsive and major histocompatibility complex-deficient tumors.[70] Additionally, a recent study showed that the phenotype, proliferative capacity, and requirement for $CD4^+$ T cells during CAR T cell production *in vitro* are important to increase persistence and mediate better tumor control *in vivo*.[71] These more favorable outcomes with enhanced therapeutic efficacy are

associated with increased persistence of CAR T cells and an increased memory T cell pool, resulting in increased proliferative capacity and long-term persistence *in vivo*. Unlike other T helper subsets, Th9 cells have unique properties because they can recruit monocytes and effectively lead to the clearance of tumor antigen loss variants through the induction of host immunity.[58] Therefore, it could be proposed as a solution to overcome the challenges faced by CAR utilizing $CD8^+$ cytotoxic effector T cells, including difficulties in impaired T cell trafficking and the immunosuppressive tumor microenvironment, leading to T cell exhaustion and poor expansion.[72] These findings prompted us to develop CD97-targeting CAR Th9 cells and subsequently observe their antitumor effects.

As the precise contribution of CD97-targeting CAR Th9 cell-mediated cytotoxicity activity, we investigated CD107a, known as lysosomal-associated membrane protein-1, which has been described as a marker of immune cell degranulation.[59] Degranulation serves as an essential prerequisite for perforin-granzyme-mediated killing and is a crucial component of the immediate lytic function exhibited by antigen-specific immune cells, including natural killer, $CD8^+$, and $CD4^+$ T cells.[59,73] CD97-targeting CAR Th9 cells induced the increase and maintenance of $CD4^+CD107a^+$ cells 7 days after injection into the tumor. However, additional research is necessary to fully understand the underlying molecular mechanisms. These CAR Th9 cells might be delivered in multiple doses over time to titrate the desired effect with fewer side effects. The dose of cytotoxic CAR Th9 cells might also be titrated based on need, and further studies are needed.[74,75]

Indeed, the potential of CD97-CAR T cells to target cancer stem cells (CSCs) in a variety of tumor types is a promising area of research that merits exploration. CD97 is not only overexpressed in GBM but also in several other malignancies, including, but not limited to, breast,[76] pancreas,[24] and prostate cancers[77] where CSCs play a pivotal role in tumor progression, metastasis, and therapy resistance. The utility of CD97-CAR T therapy in targeting CSCs across these diverse tumor types could revolutionize the approach to cancer treatment, offering a more promising and potentially curative strategy. This would be particularly relevant for aggressive and recurrent tumors, where conventional therapies fail to eliminate CSCs, leading to relapse and poor prognosis. Exploring the efficacy and specificity of CD97-CAR T cells in various cancer models could shed light on their potential as a versatile and powerful therapeutic tool against a broad spectrum of tumors.

Overall, this study suggests that CD97 serves as a functional surface antigen for GSCs. An important implication of these findings is that studies aimed at discovering therapeutic targets for GBM should not rely solely on identifying GSCs, and the targets must have functions that significantly contribute to self-renewal and tumorigenesis via CD97-related mTORC2 signaling. Moreover, $CD97^{high}$ GSCs are a conserved requirement for aggressive tumorigenic properties, thus underscoring the importance of CD97 as a potential therapeutic target. This study directly informs a clinical development strategy for CD97-targeting CAR Th9 cell therapy and reveals the strengths of targeting CD97. Thus, our study illustrates how CD97 might influence the biology of GSCs and offers a potential approach to targeted therapy for GBM.

Limitations of the study

While our study identifies CD97 as a promising target for GBM therapy, several limitations should be considered. First, the therapeutic efficacy and safety of CD97-CAR Th9 cells were demonstrated *in vitro* and in mouse models; thus, their effectiveness in humans remains uncertain. Second, although CD97 expression was consistent across the patient-derived GSCs we tested, GBM is a highly heterogeneous disease, and CD97 expression may vary among different patients. Third, the long-term impact of mTORC2 inhibition on GSCs and normal cells was not explored, nor were possible resistance mechanisms that could arise with treatment. Future studies should address these limitations by evaluating the clinical applicability and long-term effects of CD97-targeted therapies in diverse patient populations.

RESOURCE AVAILABILITY

Lead contact

Further information and requests for resources and reagents should be directed to and will be fulfilled by the lead contact, Jinlong Yin (jlyin@henu.edu.cn).

Materials availability

All materials and reagents used in this study are available from the lead contact upon request.

Data and code availability

- RNA-seq data have been deposited at Gene Expression Omnibus and are publicly available as of the date of publication. Accession numbers are listed in the key resources table.
- This paper does not report original code.
- Any additional information required to reanalyze the data reported in this work paper is available from the lead contact upon request.

ACKNOWLEDGMENTS

The authors would like to extend special thanks to Xun Jin (Tianjin Medical University Cancer Institute and Hospital) for providing GSC428 and to Rongjun Qian (Henan Provincial People's Hospital) for supplying GBM patient samples. This work was supported by grants from the National Natural Science Foundation of China (82173228) and Project of Basic Research Fund of Henan Institute of Medical and Pharmacological Sciences (2024BP0206). Cartoons in Figures 1A, 5A, 6I, and 7A were created with BioRender.com.

AUTHOR CONTRIBUTIONS

J.Y. conceived the study and supervised the project with contributions from B.S. S.Z., W.L., R.N., Z.Y., Q.Z., M.G., S.S.K., Y.D., M.L., and S.I.C. performed the experiments and analyzed the results. S.Z., W.L., X.J., S.I.C., and J.Y. wrote the manuscript. X.J. performed the bioinformatics analysis. T.C. performed mCD97 CAR cloning. S.Z., W.L., X.J., J.B.P., S.I.C., B.S., and J.Y. discussed the data and reviewed the manuscript.

DECLARATION OF INTERESTS

The authors declare no competing interests.

STAR★METHODS

Detailed methods are provided in the online version of this paper and include the following:

- KEY RESOURCES TABLE
- EXPERIMENTAL MODEL AND SUBJECT DETAILS
  - Cell lines and cell culture

- *In vivo* animal model
- Human GBM tissue and healthy blood samples

- METHOD DETAILS
  - Screening of cell-surface markers
  - Lentivirus production and infection
  - Quantitative reverse transcription-polymerase chain reaction (RT-qPCR)
  - Immunoblot analysis (IB)
  - Flow cytometry
  - PI staining and annexin V staining
  - Cell proliferation assays
  - LDAs
  - Inhibitor treatment
  - Mice models
  - Immunofluorescence (IF) staining
  - Bioinformatics analysis
  - Analysis of RNA-sequencing data
  - CAR T cell manufacturing and transduction
  - Generation of murine CAR-T cells
  - Fluorescence assay of viable cells
  - Cytotoxicity assay
  - Isolation of tumor-infiltrating immune cells
- QUANTIFICATION AND STATISTICAL ANALYSIS

SUPPLEMENTAL INFORMATION

Supplemental information can be found online at https://doi.org/10.1016/j.xcrm.2024.101844.

Received: December 12, 2023
Revised: August 19, 2024
Accepted: November 6, 2024
Published: December 4, 2024

REFERENCES

1. Louis, D.N., Perry, A., Wesseling, P., Brat, D.J., Cree, I.A., Figarella-Branger, D., Hawkins, C., Ng, H.K., Pfister, S.M., Reifenberger, G., et al. (2021). The 2021 WHO Classification of Tumors of the Central Nervous System: a summary. Neuro Oncol. *23*, 1231–1251. https://doi.org/10.1093/neuonc/noab106.
2. McKinnon, C., Nandhabalan, M., Murray, S.A., and Plaha, P. (2021). Glioblastoma: clinical presentation, diagnosis, and management. Bmj *374*, n1560. https://doi.org/10.1136/bmj.n1560.
3. Gilbertson, R.J., and Rich, J.N. (2007). Making a tumour's bed: glioblastoma stem cells and the vascular niche. Nat. Rev. Cancer *7*, 733–736. https://doi.org/10.1038/nrc2246.
4. FDA (2017). FDA approves axicabtagene ciloleucel for large B-cell lymphoma. https://www.fda.gov/drugs/resources-information-approved-drugs/fda-approves-axicabtagene-ciloleucel-large-b-cell-lymphoma.
5. Brown, C.E., Alizadeh, D., Starr, R., Weng, L., Wagner, J.R., Naranjo, A., Ostberg, J.R., Blanchard, M.S., Kilpatrick, J., Simpson, J., et al. (2016). Regression of Glioblastoma after Chimeric Antigen Receptor T-Cell Therapy. N. Engl. J. Med. *375*, 2561–2569. https://doi.org/10.1056/NEJMoa1610497.
6. O'Rourke, D.M., Nasrallah, M.P., Desai, A., Melenhorst, J.J., Mansfield, K., Morrissette, J.J.D., Martinez-Lage, M., Brem, S., Maloney, E., Shen, A., et al. (2017). A single dose of peripherally infused EGFRvIII-directed CAR T cells mediates antigen loss and induces adaptive resistance in patients with recurrent glioblastoma. Sci. Transl. Med. *9*, eaaa0984. https://doi.org/10.1126/scitranslmed.aaa0984.
7. Ahmed, N., Brawley, V., Hegde, M., Bielamowicz, K., Kalra, M., Landi, D., Robertson, C., Gray, T.L., Diouf, O., Wakefield, A., et al. (2017). HER2-Specific Chimeric Antigen Receptor-Modified Virus-Specific T Cells for Progressive Glioblastoma: A Phase 1 Dose-Escalation Trial. JAMA Oncol. *3*, 1094–1101. https://doi.org/10.1001/jamaoncol.2017.0184.
8. Singh, S.K., Clarke, I.D., Terasaki, M., Bonn, V.E., Hawkins, C., Squire, J., and Dirks, P.B. (2003). Identification of a cancer stem cell in human brain tumors. Cancer Res. *63*, 5821–5828.
9. Singh, S.K., Hawkins, C., Clarke, I.D., Squire, J.A., Bayani, J., Hide, T., Henkelman, R.M., Cusimano, M.D., and Dirks, P.B. (2004). Identification of human brain tumour initiating cells. Nature *432*, 396–401. https://doi.org/10.1038/nature03128.
10. Liu, G., Yuan, X., Zeng, Z., Tunici, P., Ng, H., Abdulkadir, I.R., Lu, L., Irvin, D., Black, K.L., and Yu, J.S. (2006). Analysis of gene expression and chemoresistance of CD133+ cancer stem cells in glioblastoma. Mol. Cancer *5*, 67. https://doi.org/10.1186/1476-4598-5-67.
11. Xu, Y., Stamenkovic, I., and Yu, Q. (2010). CD44 attenuates activation of the hippo signaling pathway and is a prime therapeutic target for glioblastoma. Cancer Res. *70*, 2455–2464. https://doi.org/10.1158/0008-5472.CAN-09-2505.
12. Anido, J., Sáez-Borderías, A., Gonzàlez-Juncà, A., Rodón, L., Folch, G., Carmona, M.A., Prieto-Sánchez, R.M., Barba, I., Martínez-Sáez, E., Prudkin, L., et al. (2010). TGF-β Receptor Inhibitors Target the CD44(high)/Id1(-high) Glioma-Initiating Cell Population in Human Glioblastoma. Cancer Cell *18*, 655–668. https://doi.org/10.1016/j.ccr.2010.10.023.
13. Son, M.J., Woolard, K., Nam, D.H., Lee, J., and Fine, H.A. (2009). SSEA-1 is an enrichment marker for tumor-initiating cells in human glioblastoma. Cell Stem Cell *4*, 440–452. https://doi.org/10.1016/j.stem.2009.03.003.
14. Erhart, F., Blauensteiner, B., Zirkovits, G., Printz, D., Soukup, K., Klingenbrunner, S., Fischhuber, K., Reitermaier, R., Halfmann, A., Lötsch, D., et al. (2019). Gliomasphere marker combinatorics: multidimensional flow cytometry detects CD44+/CD133+/ITGA6+/CD36+ signature. J. Cell Mol. Med. *23*, 281–292. https://doi.org/10.1111/jcmm.13927.
15. Li, D., Tian, Y., Hu, Y., Qi, Y., Tian, N., Li, S., Hu, P., Wu, F., Wei, Q., Wei, Z., et al. (2019). Glioma-associated human endothelial cell-derived extracellular vesicles specifically promote the tumourigenicity of glioma stem cells via CD9. Oncogene *38*, 6898–6912. https://doi.org/10.1038/s41388-019-0903-6.
16. Bao, S., Wu, Q., Li, Z., Sathornsumetee, S., Wang, H., McLendon, R.E., Hjelmeland, A.B., and Rich, J.N. (2008). Targeting cancer stem cells through L1CAM suppresses glioma growth. Cancer Res. *68*, 6043–6048. https://doi.org/10.1158/0008-5472.CAN-08-1079.
17. Lathia, J.D., Li, M., Sinyuk, M., Alvarado, A.G., Flavahan, W.A., Stoltz, K., Rosager, A.M., Hale, J., Hitomi, M., Gallagher, J., et al. (2014). High-throughput flow cytometry screening reveals a role for junctional adhesion molecule a as a cancer stem cell maintenance factor. Cell Rep. *6*, 117–129. https://doi.org/10.1016/j.celrep.2013.11.043.
18. Lathia, J.D., Gallagher, J., Heddleston, J.M., Wang, J., Eyler, C.E., Macswords, J., Wu, Q., Vasanji, A., McLendon, R.E., Hjelmeland, A.B., and Rich, J.N. (2010). Integrin alpha 6 regulates glioblastoma stem cells. Cell Stem Cell *6*, 421–432. https://doi.org/10.1016/j.stem.2010.02.018.
19. Vora, P., Venugopal, C., Salim, S.K., Tatari, N., Bakhshinyan, D., Singh, M., Seyfrid, M., Upreti, D., Rentas, S., Wong, N., et al. (2020). The Rational Development of CD133-Targeting Immunotherapies for Glioblastoma. Cell Stem Cell *26*, 832–844.e6. https://doi.org/10.1016/j.stem.2020.04.008.
20. Kieliszek, A.M., Mobilio, D., Upreti, D., Bloemberg, D., Escudero, L., Kwiecien, J.M., Alizada, Z., Zhai, K., Ang, P., Chafe, S.C., et al. (2024). Intratumoral Delivery of Chimeric Antigen Receptor T Cells Targeting CD133 Effectively Treats Brain Metastases. Clin. Cancer Res. *30*, 554–563. https://doi.org/10.1158/1078-0432.Ccr-23-1735.
21. Prater, K.E., Aloi, M.S., Pathan, J.L., Winston, C.N., Chernoff, R.A., Davidson, S., Sadgrove, M., McDonough, A., Zierath, D., Su, W., et al. (2021). A Subpopulation of Microglia Generated in the Adult Mouse Brain Originates from Prominin-1-Expressing Progenitors. J. Neurosci. *41*, 7942–7953. https://doi.org/10.1523/jneurosci.1893-20.2021.

22. Hamann, J., Eichler, W., Hamann, D., Kerstens, H.M., Poddighe, P.J., Hoovers, J.M., Hartmann, E., Strauss, M., and van Lier, R.A. (1995). Expression cloning and chromosomal mapping of the leukocyte activation antigen CD97, a new seven-span transmembrane molecule of the secretion receptor superfamily with an unusual extracellular domain. J. Immunol. *155*, 1942–1950.

23. Martin, G.H., Roy, N., Chakraborty, S., Desrichard, A., Chung, S.S., Woolthuis, C.M., Hu, W., Berezniuk, I., Garrett-Bakelman, F.E., Hamann, J., et al. (2019). CD97 is a critical regulator of acute myeloid leukemia stem cell function. J. Exp. Med. *216*, 2362–2377. https://doi.org/10.1084/jem.20190598.

24. Ward, Y., Lake, R., Martin, P.L., Killian, K., Salerno, P., Wang, T., Meltzer, P., Merino, M., Cheng, S.Y., Santoro, M., et al. (2013). CD97 amplifies LPA receptor signaling and promotes thyroid cancer progression in a mouse model. Oncogene *32*, 2726–2738. https://doi.org/10.1038/onc.2012.301.

25. Yin, Y., Xu, X., Tang, J., Zhang, W., Zhangyuan, G., Ji, J., Deng, L., Lu, S., Zhuo, H., and Sun, B. (2018). CD97 Promotes Tumor Aggressiveness Through the Traditional G Protein-Coupled Receptor-Mediated Signaling in Hepatocellular Carcinoma. Hepatology *68*, 1865–1878. https://doi.org/10.1002/hep.30068.

26. Hilbig, D., Dietrich, N., Wandel, E., Gonsior, S., Sittig, D., Hamann, J., and Aust, G. (2018). The Interaction of CD97/ADGRE5 With beta-Catenin in Adherens Junctions Is Lost During Colorectal Carcinogenesis. Front. Oncol. *8*, 182. https://doi.org/10.3389/fonc.2018.00182.

27. He, Z., Wu, H., Jiao, Y., and Zheng, J. (2015). Expression and prognostic value of CD97 and its ligand CD55 in pancreatic cancer. Oncol. Lett. *9*, 793–797. https://doi.org/10.3892/ol.2014.2751.

28. Chidambaram, A., Fillmore, H.L., Van Meter, T.E., Dumur, C.I., and Broaddus, W.C. (2012). Novel report of expression and function of CD97 in malignant gliomas: correlation with Wilms tumor 1 expression and glioma cell invasiveness. J. Neurosurg. *116*, 843–853. https://doi.org/10.3171/2011.11.JNS111455.

29. Safaee, M., Clark, A.J., Oh, M.C., Ivan, M.E., Bloch, O., Kaur, G., Sun, M.Z., Kim, J.M., Oh, T., Berger, M.S., and Parsa, A.T. (2013). Overexpression of CD97 confers an invasive phenotype in glioblastoma cells and is associated with decreased survival of glioblastoma patients. PLoS One *8*, e62765. https://doi.org/10.1371/journal.pone.0062765.

30. Liu, J.K., Lubelski, D., Schonberg, D.L., Wu, Q., Hale, J.S., Flavahan, W.A., Mulkearns-Hubert, E.E., Man, J., Hjelmeland, A.B., Yu, J., et al. (2014). Phage display discovery of novel molecular targets in glioblastoma-initiating cells. Cell Death Differ. *21*, 1325–1339. https://doi.org/10.1038/cdd.2014.65.

31. Somasundaram, A., Ardanowski, N., Opalak, C.F., Fillmore, H.L., Chidambaram, A., and Broaddus, W.C. (2014). Wilms tumor 1 gene, CD97, and the emerging biogenetic profile of glioblastoma. Neurosurg. Focus *37*, E14. https://doi.org/10.3171/2014.9.FOCUS14506.

32. Mallawaaratchy, D.M., Buckland, M.E., McDonald, K.L., Li, C.C.Y., Ly, L., Sykes, E.K., Christopherson, R.I., and Kaufman, K.L. (2015). Membrane proteome analysis of glioblastoma cell invasion. J. Neuropathol. Exp. Neurol. *74*, 425–441. https://doi.org/10.1097/NEN.0000000000000187.

33. Safaee, M., Fakurnejad, S., Bloch, O., Clark, A.J., Ivan, M.E., Sun, M.Z., Oh, T., Phillips, J.J., and Parsa, A.T. (2015). Proportional upregulation of CD97 isoforms in glioblastoma and glioblastoma-derived brain tumor initiating cells. PLoS One *10*, e0111532. https://doi.org/10.1371/journal.pone.0111532.

34. Eichberg, D.G., Slepak, T.I., Pascoini, A.L., Komotar, R.J., and Ivan, M.E. (2021). Genetic manipulation of adhesion GPCR CD97/ADGRE5 modulates invasion in patient-derived glioma stem cells. J. Neuro Oncol. *153*, 383–391. https://doi.org/10.1007/s11060-021-03778-8.

35. Safaee, M.M., Wang, E.J., Jain, S., Chen, J.S., Gill, S., Zheng, A.C., Garcia, J.H., Beniwal, A.S., Tran, Y., Nguyen, A.T., et al. (2022). CD97 is associated with mitogenic pathway activation, metabolic reprogramming, and immune microenvironment changes in glioblastoma. Sci. Rep. *12*, 1464. https://doi.org/10.1038/s41598-022-05259-y.

36. Ravn-Boess, N., Roy, N., Hattori, T., Bready, D., Donaldson, H., Lawson, C., Lapierre, C., Korman, A., Rodrick, T., Liu, E., et al. (2023). The expression profile and tumorigenic mechanisms of CD97 (ADGRE5) in glioblastoma render it a targetable vulnerability. Cell Rep. *42*, 113374. https://doi.org/10.1016/j.celrep.2023.113374.

37. Slepak, T.I., Guyot, M., Walters, W., Eichberg, D.G., and Ivan, M.E. (2023). Dual role of the adhesion G-protein coupled receptor ADRGE5/CD97 in glioblastoma invasion and proliferation. J. Biol. Chem. *299*, 105105. https://doi.org/10.1016/j.jbc.2023.105105.

38. Wang, L.B., Karpova, A., Gritsenko, M.A., Kyle, J.E., Cao, S., Li, Y., Rykunov, D., Colaprico, A., Rothstein, J.H., Hong, R., et al. (2021). Proteogenomic and metabolomic characterization of human glioblastoma. Cancer Cell *39*, 509–528.e20. https://doi.org/10.1016/j.ccell.2021.01.006.

39. Wang, Q., Hu, B., Hu, X., Kim, H., Squatrito, M., Scarpace, L., deCarvalho, A.C., Lyu, S., Li, P., Li, Y., et al. (2017). Tumor Evolution of Glioma-Intrinsic Gene Expression Subtypes Associates with Immunological Changes in the Microenvironment. Cancer Cell *32*, 42–56.e6. https://doi.org/10.1016/j.ccell.2017.06.003.

40. Restall, I.J., Cseh, O., Richards, L.M., Pugh, T.J., Luchman, H.A., and Weiss, S. (2020). Brain Tumor Stem Cell Dependence on Glutaminase Reveals a Metabolic Vulnerability through the Amino Acid Deprivation Response Pathway. Cancer Res. *80*, 5478–5490. https://doi.org/10.1158/0008-5472.CAN-19-3923.

41. Richards, L.M., Whitley, O.K.N., MacLeod, G., Cavalli, F.M.G., Coutinho, F.J., Jaramillo, J.E., Svergun, N., Riverin, M., Croucher, D.C., Kushida, M., et al. (2021). Gradient of Developmental and Injury Response transcriptional states defines functional vulnerabilities underpinning glioblastoma heterogeneity. Nat. Cancer *2*, 157–173. https://doi.org/10.1038/s43018-020-00154-9.

42. Strojnik, T., Røsland, G.V., Sakariassen, P.O., Kavalar, R., and Lah, T. (2007). Neural stem cell markers, nestin and musashi proteins, in the progression of human glioma: correlation of nestin with prognosis of patient survival. Surg. Neurol. *68*, 133–143, discussion 143-134. https://doi.org/10.1016/j.surneu.2006.10.050.

43. Gangemi, R.M.R., Griffero, F., Marubbi, D., Perera, M., Capra, M.C., Malatesta, P., Ravetti, G.L., Zona, G.L., Daga, A., and Corte, G. (2009). SOX2 silencing in glioblastoma tumor-initiating cells causes stop of proliferation and loss of tumorigenicity. Stem Cell. *27*, 40–48. https://doi.org/10.1634/stemcells.2008-0493.

44. Zbinden, M., Duquet, A., Lorente-Trigos, A., Ngwabyt, S.N., Borges, I., and Ruiz i Altaba, A. (2010). NANOG regulates glioma stem cells and is essential in vivo acting in a cross-functional network with GLI1 and p53. EMBO J. *29*, 2659–2674. https://doi.org/10.1038/emboj.2010.137.

45. Lopez-Bertoni, H., Lal, B., Li, A., Caplan, M., Guerrero-Cázares, H., Eberhart, C.G., Quiñones-Hinojosa, A., Glas, M., Scheffler, B., Laterra, J., and Li, Y. (2015). DNMT-dependent suppression of microRNA regulates the induction of GBM tumor-propagating phenotype by Oct4 and Sox2. Oncogene *34*, 3994–4004. https://doi.org/10.1038/onc.2014.334.

46. Beier, D., Hau, P., Proescholdt, M., Lohmeier, A., Wischhusen, J., Oefner, P.J., Aigner, L., Brawanski, A., Bogdahn, U., and Beier, C.P. (2007). CD133(+) and CD133(-) glioblastoma-derived cancer stem cells show differential growth characteristics and molecular profiles. Cancer Res. *67*, 4010–4015. https://doi.org/10.1158/0008-5472.CAN-06-4180.

47. Alcantara Llaguno, S., and Parada, L.F. (2021). Cancer stem cells in gliomas: evolving concepts and therapeutic implications. Curr. Opin. Neurol. *34*, 868–874. https://doi.org/10.1097/WCO.0000000000000994.

48. Carracedo, A., Ma, L., Teruya-Feldstein, J., Rojo, F., Salmena, L., Alimonti, A., Egia, A., Sasaki, A.T., Thomas, G., Kozma, S.C., et al. (2008). Inhibition of mTORC1 leads to MAPK pathway activation through a PI3K-dependent feedback loop in human cancer. J. Clin. Invest. *118*, 3065–3074. https://doi.org/10.1172/JCI34739.

49. Palm, W., Park, Y., Wright, K., Pavlova, N.N., Tuveson, D.A., and Thompson, C.B. (2015). The Utilization of Extracellular Proteins as Nutrients Is

Suppressed by mTORC1. Cell *162*, 259–270. https://doi.org/10.1016/j.cell.2015.06.017.

50. Sarbassov, D.D., Guertin, D.A., Ali, S.M., and Sabatini, D.M. (2005). Phosphorylation and regulation of Akt/PKB by the rictor-mTOR complex. Science *307*, 1098–1101. https://doi.org/10.1126/science.1106148.
51. Sommer, E.M., Dry, H., Cross, D., Guichard, S., Davies, B.R., and Alessi, D.R. (2013). Elevated SGK1 predicts resistance of breast cancer cells to Akt inhibitors. Biochem. J. *452*, 499–508. https://doi.org/10.1042/BJ20130342.
52. Gasser, J.A., Inuzuka, H., Lau, A.W., Wei, W., Beroukhim, R., and Toker, A. (2014). SGK3 mediates INPP4B-dependent PI3K signaling in breast cancer. Mol. Cell *56*, 595–607. https://doi.org/10.1016/j.molcel.2014.09.023.
53. Dong, R., Libby, K.A., Blaeschke, F., Fuchs, W., Marson, A., Vale, R.D., and Su, X. (2020). Rewired signaling network in T cells expressing the chimeric antigen receptor (CAR). EMBO J. *39*, e104730. https://doi.org/10.15252/embj.2020104730.
54. Gudipati, V., Rydzek, J., Doel-Perez, I., Gonçalves, V.D.R., Scharf, L., Königsberger, S., Lobner, E., Kunert, R., Einsele, H., Stockinger, H., et al. (2020). Inefficient CAR-proximal signaling blunts antigen sensitivity. Nat. Immunol. *21*, 848–856. https://doi.org/10.1038/s41590-020-0719-0.
55. Majzner, R.G., Rietberg, S.P., Sotillo, E., Dong, R., Vachharajani, V.T., Labanieh, L., Myklebust, J.H., Kadapakkam, M., Weber, E.W., Tousley, A.M., et al. (2020). Tuning the Antigen Density Requirement for CAR T-cell Activity. Cancer Discov. *10*, 702–723. https://doi.org/10.1158/2159-8290.CD-19-0945.
56. Lu, Y., Wang, Q., Xue, G., Bi, E., Ma, X., Wang, A., Qian, J., Dong, C., and Yi, Q. (2018). Th9 Cells Represent a Unique Subset of CD4(+) T Cells Endowed with the Ability to Eradicate Advanced Tumors. Cancer Cell *33*, 1048–1060.e7. https://doi.org/10.1016/j.ccell.2018.05.004.
57. Speiser, D.E., Chijioke, O., Schaeuble, K., and Münz, C. (2023). CD4(+) T cells in cancer. Nat. Cancer *4*, 317–329. https://doi.org/10.1038/s43018-023-00521-2.
58. Xue, G., Zheng, N., Fang, J., Jin, G., Li, X., Dotti, G., Yi, Q., and Lu, Y. (2021). Adoptive cell therapy with tumor-specific Th9 cells induces viral mimicry to eliminate antigen-loss-variant tumor cells. Cancer Cell *39*, 1610–1622.e9. https://doi.org/10.1016/j.ccell.2021.09.011.
59. Tian, Y., Sette, A., and Weiskopf, D. (2016). Cytotoxic CD4 T Cells: Differentiation, Function, and Application to Dengue Virus Infection. Front. Immunol. *7*, 531. https://doi.org/10.3389/fimmu.2016.00531.
60. Brown, C.E., Hibbard, J.C., Alizadeh, D., Blanchard, M.S., Natri, H.M., Wang, D., Ostberg, J.R., Aguilar, B., Wagner, J.R., Paul, J.A., et al. (2024). Locoregional delivery of IL-13Rα2-targeting CAR-T cells in recurrent high-grade glioma: a phase 1 trial. Nat. Med. *30*, 1001–1012. https://doi.org/10.1038/s41591-024-02875-1.
61. Donovan, L.K., Delaidelli, A., Joseph, S.K., Bielamowicz, K., Fousek, K., Holgado, B.L., Manno, A., Srikanthan, D., Gad, A.Z., Van Ommeren, R., et al. (2020). Locoregional delivery of CAR T cells to the cerebrospinal fluid for treatment of metastatic medulloblastoma and ependymoma. Nat. Med. *26*, 720–731. https://doi.org/10.1038/s41591-020-0827-2.
62. Du, H., Hirabayashi, K., Ahn, S., Kren, N.P., Montgomery, S.A., Wang, X., Tiruthani, K., Mirlekar, B., Michaud, D., Greene, K., et al. (2019). Antitumor Responses in the Absence of Toxicity in Solid Tumors by Targeting B7-H3 via Chimeric Antigen Receptor T Cells. Cancer Cell *35*, 221–237.e8. https://doi.org/10.1016/j.ccell.2019.01.002.
63. Zheng, N., Fang, J., Xue, G., Wang, Z., Li, X., Zhou, M., Jin, G., Rahman, M.M., McFadden, G., and Lu, Y. (2022). Induction of tumor cell autosis by myxoma virus-infected CAR-T and TCR-T cells to overcome primary and acquired resistance. Cancer Cell *40*, 973–985.e7. https://doi.org/10.1016/j.ccell.2022.08.001.
64. Dirks, P.B. (2008). Brain tumour stem cells: the undercurrents of human brain cancer and their relationship to neural stem cells. Philos. Trans. R. Soc. Lond. B Biol. Sci. *363*, 139–152. https://doi.org/10.1098/rstb.2006.2017.
65. Galdieri, L., Jash, A., Malkova, O., Mao, D.D., DeSouza, P., Chu, Y.E., Salter, A., Campian, J.L., Naegle, K.M., Brennan, C.W., et al. (2021). Defining phenotypic and functional heterogeneity of glioblastoma stem cells by mass cytometry. JCI Insight *6*, e128456. https://doi.org/10.1172/jci.insight.128456.
66. Hatakeyama, J., Wald, J.H., Printsev, I., Ho, H.Y.H., and Carraway, K.L., 3rd. (2014). Vangl1 and Vangl2: planar cell polarity components with a developing role in cancer. Endocr. Relat. Cancer *21*, R345–R356. https://doi.org/10.1530/erc-14-0141.
67. Ghosh, S., Mukherjee, S., Sengupta, A., Chowdhury, S., Sarkar, S., Keswani, T., and Bhattacharyya, A. (2022). CD4(+)IL9(+) (Th9) cells as the major source of IL-9, potentially modulate Th17/Treg mediated host immune response during experimental cerebral malaria. Mol. Immunol. *152*, 240–254. https://doi.org/10.1016/j.molimm.2022.11.005.
68. Gomes-Silva, D., Srinivasan, M., Sharma, S., Lee, C.M., Wagner, D.L., Davis, T.H., Rouce, R.H., Bao, G., Brenner, M.K., and Mamonkin, M. (2017). CD7-edited T cells expressing a CD7-specific CAR for the therapy of T-cell malignancies. Blood *130*, 285–296. https://doi.org/10.1182/blood-2017-01-761320.
69. Chen, D., Varanasi, S.K., Hara, T., Traina, K., Sun, M., McDonald, B., Farsakoglu, Y., Clanton, J., Xu, S., Garcia-Rivera, L., et al. (2023). CTLA-4 blockade induces a microglia-Th1 cell partnership that stimulates microglia phagocytosis and anti-tumor function in glioblastoma. Immunity *56*, 2086–2104.e8. https://doi.org/10.1016/j.immuni.2023.07.015.
70. Kruse, B., Buzzai, A.C., Shridhar, N., Braun, A.D., Gellert, S., Knauth, K., Pozniak, J., Peters, J., Dittmann, P., Mengoni, M., et al. (2023). CD4(+) T cell-induced inflammatory cell death controls immune-evasive tumours. Nature *618*, 1033–1040. https://doi.org/10.1038/s41586-023-06199-x.
71. Meyran, D., Zhu, J.J., Butler, J., Tantalo, D., MacDonald, S., Nguyen, T.N., Wang, M., Thio, N., D'Souza, C., Qin, V.M., et al. (2023). T(STEM)-like CAR-T cells exhibit improved persistence and tumor control compared with conventional CAR-T cells in preclinical models. Sci. Transl. Med. *15*, eabk1900. https://doi.org/10.1126/scitranslmed.abk1900.
72. Choi, S.I., and Yin, J. (2022). Prospective approaches to enhancing CAR T cell therapy for glioblastoma. Front. Immunol. *13*, 1008751. https://doi.org/10.3389/fimmu.2022.1008751.
73. Cohnen, A., Chiang, S.C., Stojanovic, A., Schmidt, H., Claus, M., Saftig, P., Janßen, O., Cerwenka, A., Bryceson, Y.T., and Watzl, C. (2013). Surface CD107a/LAMP-1 protects natural killer cells from degranulation-associated damage. Blood *122*, 1411–1418. https://doi.org/10.1182/blood-2012-07-441832.
74. Aghajanian, H., Rurik, J.G., and Epstein, J.A. (2022). CAR-based therapies: opportunities for immuno-medicine beyond cancer. Nat. Metab. *4*, 163–169. https://doi.org/10.1038/s42255-022-00537-5.
75. Milone, M.C., Xu, J., Chen, S.J., Collins, M.A., Zhou, J., Powell, D.J., Jr., and Melenhorst, J.J. (2021). Engineering enhanced CAR T-cells for improved cancer therapy. Nat. Cancer *2*, 780–793. https://doi.org/10.1038/s43018-021-00241-5.
76. Aust, G., Zheng, L., and Quaas, M. (2022). To Detach, Migrate, Adhere, and Metastasize: CD97/ADGRE5 in Cancer. Cells *11*, 1538. https://doi.org/10.3390/cells11091538.
77. Ward, Y., Lake, R., Yin, J.J., Heger, C.D., Raffeld, M., Goldsmith, P.K., Merino, M., and Kelly, K. (2011). LPA receptor heterodimerizes with CD97 to amplify LPA-initiated RHO-dependent signaling and invasion in prostate cancer cells. Cancer Res. *71*, 7301–7311. https://doi.org/10.1158/0008-5472.Can-11-2381.
78. Walter, D.M., Venancio, O.S., Buza, E.L., Tobias, J.W., Deshpande, C., Gudiel, A.A., Kim-Kiselak, C., Cicchini, M., Yates, T.J., and Feldser, D.M. (2017). Systematic In Vivo Inactivation of Chromatin-Regulating Enzymes Identifies Setd2 as a Potent Tumor Suppressor in Lung Adenocarcinoma. Cancer Res. *77*, 1719–1729. https://doi.org/10.1158/0008-5472.Can-16-2159.
79. Lin, W., Niu, R., Park, S.M., Zou, Y., Kim, S.S., Xia, X., Xing, S., Yang, Q., Sun, X., Yuan, Z., et al. (2023). IGFBP5 is an ROR1 ligand promoting

glioblastoma invasion via ROR1/HER2-CREB signaling axis. Nat. Commun. *14*, 1578. https://doi.org/10.1038/s41467-023-37306-1.

80. Yin, J., Kim, S.S., Choi, E., Oh, Y.T., Lin, W., Kim, T.H., Sa, J.K., Hong, J.H., Park, S.H., Kwon, H.J., et al. (2020). ARS2/MAGL signaling in glioblastoma stem cells promotes self-renewal and M2-like polarization of tumor-associated macrophages. Nat. Commun. *11*, 2978. https://doi.org/10.1038/s41467-020-16789-2.

81. Patel, A.P., Tirosh, I., Trombetta, J.J., Shalek, A.K., Gillespie, S.M., Wakimoto, H., Cahill, D.P., Nahed, B.V., Curry, W.T., Martuza, R.L., et al. (2014). Single-cell RNA-seq highlights intratumoral heterogeneity in primary glioblastoma. Science *344*, 1396–1401. https://doi.org/10.1126/science.1254257.

82. Yin, J., Jung, J.E., Choi, S.I., Kim, S.S., Oh, Y.T., Kim, T.H., Choi, E., Lee, S.J., Kim, H., Kim, E.O., et al. (2018). Inhibition of BMP signaling overcomes acquired resistance to cetuximab in oral squamous cell carcinomas. Cancer Lett. *414*, 181–189. https://doi.org/10.1016/j.canlet.2017.11.013.

83. Verhaak, R.G.W., Hoadley, K.A., Purdom, E., Wang, V., Qi, Y., Wilkerson, M.D., Miller, C.R., Ding, L., Golub, T., Mesirov, J.P., et al. (2010). Integrated genomic analysis identifies clinically relevant subtypes of glioblastoma characterized by abnormalities in PDGFRA, IDH1, EGFR, and NF1. Cancer Cell *17*, 98–110. https://doi.org/10.1016/j.ccr.2009.12.020.

84. (2008). Comprehensive genomic characterization defines human glioblastoma genes and core pathways. Nature *455*, 1061–1068. https://doi.org/10.1038/nature07385.

85. Wang, Y., Qian, T., You, G., Peng, X., Chen, C., You, Y., Yao, K., Wu, C., Ma, J., Sha, Z., et al. (2015). Localizing seizure-susceptible brain regions associated with low-grade gliomas using voxel-based lesion-symptom mapping. Neuro Oncol. *17*, 282–288. https://doi.org/10.1093/neuonc/nou130.

86. Madhavan, S., Zenklusen, J.C., Kotliarov, Y., Sahni, H., Fine, H.A., and Buetow, K. (2009). Rembrandt: helping personalized medicine become a reality through integrative translational research. Mol. Cancer Res. *7*, 157–167. https://doi.org/10.1158/1541-7786.Mcr-08-0435.

STAR★METHODS

KEY RESOURCES TABLE

REAGENT or RESOURCE	SOURCE	IDENTIFIER
Antibodies		
Anti-CD97 antibody [EPR4427] ab108368	Abcam	Cat# ab108368; RRID: AB_10865208
Nestin	BD Biosciences	Cat# 611658; RRID: AB_399176
OCT4/POU5F1 Polyclonal antibody	Proteintech	Cat# 11263-1-AP; RRID: AB_2167545
Nanog	Sangon Biotech	Cat# D155241; RRID: AB_3661675
Phospho-p70 S6 Kinase (Ser371) Antibody	Cell Signaling Technology	Cat# 9208; RRID: AB_330990
Phospho-p70 S6 Kinase (Thr389) (108D2) Rabbit mAb	Cell Signaling Technology	Cat# 9234; RRID: AB_2269803
p70 S6 Kinase (49D7) Rabbit mAb	Cell Signaling Technology	Cat# 2708; RRID: AB_390722
Akt Antibody	Cell Signaling Technology	Cat# 9272; RRID: AB_329827
p-Akt S473	Cell Signaling Technology	Cat# 9271; RRID: AB_329825
Phospho-Akt (Thr308) (C31E5E) Rabbit mAb	Cell Signaling Technology	Cat# 2965; RRID: AB_2255933
Anti-ARHGAP1 Antibody (C-10)	Santa Cruz Biotechnology	Cat# sc-398671; RRID: AB_2924417
CD133 antibody	Proteintech	Cat# 18470-1-AP; RRID: AB_2172859
Human CD44s Pan Specific MAb (Clone 2C5)	R&D Systems	Cat# BBA10; RRID: AB_356933
Human/Mouse/Rat SOX2 Antibody	R&D Systems	Cat# AF2018; RRID: AB_355110
Anti-Vinculin antibody produced in rabbit	Sigma-Aldrich	Cat# V4139; RRID: AB_262053
β-Actin (I102) polyclonal antibody	Bioworld Technology	Cat# AP0060; RRID: AB_2797445
Anti-GAPDH rabbit polyclonal antibody	Sangon Biotech	Cat# D110016; RRID:AB_2904600
FACS: PE anti-human CD97	BioLegend	Cat# 336307; RRID: AB_1227612
FACS: Nestin Monoclonal Antibody (196908), APC	Thermo Fisher Scientific	Cat# MA5-23650; RRID: AB_2608686
FACS: Alexa Fluor(R) 647 anti-OCT4 (OCT3)	BioLegend	Cat# 653710; RRID: AB_2566689
FACS: Alexa Fluor(R) 647 anti-Nanog	BioLegend	Cat# 674010; RRID: AB_2632605
FACS: APC anti-human CD133	BioLegend	Cat# 397905; RRID: AB_2876721
FACS: Alexa Fluor(R) 488 anti-human CD44	BioLegend	Cat# 397507; RRID: AB_2876719
FACS: Alexa Fluor(R) 488 anti-human CD15 (SSEA-1)	BioLegend	Cat# 301910; RRID: AB_493257
FACS: APC anti-human/mouse CD49f	BioLegend	Cat# 313615; RRID: AB_1575047
FACS: BD Pharmingen™ APC Mouse Anti-Human IFN-γ	BD Biosciences	Cat# 554702; RRID: AB_398580
FACS: Mouse Anti-Human CD3 Monoclonal Antibody	BD Biosciences	Cat# 560176; RRID: AB_1645475
FACS: PerCP/Cyanine5.5 anti-human CD4	BioLegend	Cat# 317427; RRID: AB_1186124
FACS: PE anti-human CD107a (LAMP-1)	BioLegend	Cat# 328607; RRID: AB_1186062
BZW1 antibody	GeneTex	Cat# GTX120426; RRID: AB_2885492
BZW2 antibody	Bethyl Laboratoriess	Cat# A304-608A-T; RRID: AB_3661728
Alexa Fluor® 488-*anti*-rabbit IgG	Thermo Fisher Scientific	Cat# A-11001; RRID: AB_2534069
Alexa Fluor® 568 anti-mouse IgG	Thermo Fisher Scientific	Cat# A10042; RRID: AB_2534017
Bacterial and virus strains		
Trelief ® 5 Chemically Competent Cell	Tsingke Biotech	Cat# TSC-C01
pLKO.1-puro	Bob Weinberg Lab Materials	Addgene plasmid #8453
LentiCRISPRv2GFP	Walter et al.[78]	Addgene plasmid #82416
Biological samples		
Human peripheral blood mononuclear cells (PBMCs)	Healthy donors	N/A

(*Continued on next page*)

Continued

REAGENT or RESOURCE	SOURCE	IDENTIFIER
GBM specimens	Henan Provincial People's Hospital (Henan, China, #2020-107)	N/A
Chemicals, peptides, and recombinant proteins		
B27 supplement	Invitrogen	Cat# 17504044
Recombinant Human EGF Protein	R&D Systems	Cat# 236-EG
Recombinant Human FGF basic/FGF2/bFGF	R&D Systems	Cat# 4114-TC
containing Torin1	SelleckChem	Cat# S2827
Akt inhibitor IV	CruzCredit	Cat# sc-394003
Rapamycin	SelleckChem	Cat# S1039
JR-AB2-011	Targetmol	Cat# T11728
Purified NA/LE Mouse Anti-Human CD3	BD Biosciences	Cat# 555336; RRID: AB_395742
Purified NA/LE Mouse Anti-Human CD28	BD Biosciences	Cat# 555725; RRID: AB_396068
InVivoMAb anti-human-IFN- γ	Bio X Cell	Cat# BE0235; RRID: AB_2687717
Purified NA/LE Hamster Anti-Mouse CD3e Clone 145-2C11	BD Biosciences	Cat# 553057; RRID: AB_394590
Purified anti-mouse CD28	BioLegend	Cat# 102102; RRID: AB_312867
Recombinant Human IL-4	Novoprotein	Cat# CX03
Recombinant Human TGF-beta 1	Novoprotein	Cat# CA59
Recombinant Human IL-2	Novoprotein	Cat# C013
Human IL-2 Recombinant Protein	Peprotech	Cat# 200-02
4′,6-diamidino-2-phenylindole (DAPI, Thermo-Fisher Scientific)	Solarbio	Cat# C0065
Accutase	MPBio	Cat# 091000449
Trypsin-EDTA (0.25%)	Gibco	Cat# A11105-01
Penicilin-Streptomycin Solutions (100X)	WELGENE	Cat# LS202-02
Lipofectamine 2000	Invitrogene	Cat# 11668-019
Polybrene	Sigma	Cat# TR-1003
Paraformaldehyde (PFA)	Biosesang	Cat# PC2031
Triton X-100	Bio Basic	Cat# BT0198
RIPA buffer	Solarbio	Cat# R0020
skim milk	Epizyme	Cat# PS112L
PEG300	Targetmol	Cat# T7022
Dimethyl sulfoxide DMSO (cell culture grade)	Biosharp	Cat# BL165B
Tween-80	Sangon Biotech	Cat# A100442-0500
DMEM/F-12	WELGENE	Cat# LM-002-04
RPMI-1640 Medium	ATCC	Cat# 30-2001
Penicillin-streptomycin (10,000 U/mL)	Gibco	Cat# 15140122
NEAA Cell Culture Additive (100×)	Oricellbio	Cat# NEAA-10201-100
High Glucose DMEM	Hyclone	Cat# SH30243.01
FBS	Hyclone	Cat# SH30243.03
Ficoll-Paque plus	GE Healthcare	Cat# 17144003
Celltracker CM-DiI dye	Yeasen	Cat# 40718ES50
Critical commercial assays		
EasySep™ Human $CD4^+$ T cell Isolation Kit	STEMCELL	Cat# 17952
EasySep™ Mouse T cell Isolation Kit	STEMCELL	Cat# 19851
Fluorokinase Reporter Gene Assay Kit	Beyotime	Cat# RG005
Lenti-X concentrator	Clontech (TaKaRa)	Cat# 631232
Rneasy Mini Kit	QIAGENE	Cat# 74104
AmpiGene cDNA Synthesis Kit	Enzo	Cat# ENZ-KIT 106

(*Continued on next page*)

Continued

REAGENT or RESOURCE	SOURCE	IDENTIFIER
AmpiGene qPCR Green Mix Hi-ROX	Enzo	Cat# ENZ-NUC104-1000
Annexin V-FITC Apoptosis Assay Kit	Beyotime	Cat# C1062S
CCK-8 Cell Proliferation and Cytotoxicity Assay Kit	Solarbio	Cat# CA1210
Deposited data		
Bulk RNA-Seq data in this paper	Gene Expression Omnibus	GSE201960
Experimental models: cell lines		
Human: 83 GSC	Weiwei et al.[79]	N/A
Human: X01 GSC	Weiwei et al.[79]	N/A
Human: 528 GSC	Jinlong et al.[80]	N/A
Human: 131 GSC	Weiwei et al.[79]	N/A
Human: 448 GSC	Weiwei et al.[79]	N/A
Human: GSC211	This paper	N/A
Human: GSC924	This paper	N/A
Human: GSC028	This paper	N/A
Human: GSC428	This paper	N/A
Human: GSC772	Weiwei et al.[79]	N/A
Human: HA1800	ScienCell Research Laboratories	Cat#1800
Human: U87	ATCC	Cat# HTB-14™
Human: U251	Cellosaurus	Cat# CVCL_0021
Human: 293T	ATCC	Cat# CRL-3216™
Mouse: GL261	Neuros Creative Biolabs	CAT#: NCL-2108P28
Human: Th9 cells	This paper	N/A
Mouse: $CD3^+$T cells	This paper	N/A
Experimental models: organisms/strains		
BALB/c nude mice	SPF (Beijing) biotechnology Co. Ltd.	N/A
NTG mice	SPF (Beijing) biotechnology Co. Ltd.	N/A
C57BL/6J mice	SPF (Beijing) biotechnology Co. Ltd.	N/A
Oligonucleotides		
shRNA targeting sequence: shCtrl, CCTAAGGTTAAGTCGCCCTCG	Merck	N/A
shRNA targeting sequence: shCD97-1, GCCGAACTGGAGGAGATATAT	Merck	TRC Clone ID: TRCN0000356764
shRNA targeting sequence: shCD97-3, GCGATCCTTATGGCTCATTAT	Merck	TRC Clone ID: TRCN0000008235
PCR amplified oligomers: BZW1, sense ATAGAAGATTCTAGAGCTAGCATGAATAA TCAAAAGCAGCAAAAGC	Tsingke	N/A
PCR amplified oligomers: BZW2, sense CGGCTAGCCGATGGATCCGCTCTCAGAGCT	Tsingke	N/A
PCR amplified oligomers: ARHGAP1, sense GGCTAGCCATGAATAAGCATCAGAAGCC	Tsingke	N/A
PCR amplified oligomers: CD97, sense GCTAGCCATGGGAGGCCGCGTCTTTCT	Tsingke	N/A
sgRNA targeting sequence: sgCtrl, CGAATATTATTTCTATCGGG	Tsingke	N/A
sgRNA targeting sequence: sgCD97-1, CCTTACCTGGATGGTGACCT	Tsingke	N/A

(*Continued on next page*)

Continued

REAGENT or RESOURCE	SOURCE	IDENTIFIER
sgRNA targeting sequence: sgCD97-2, CTCCAAGACAAGCTCAGCCG	Tsingke	N/A
Primers for CD97, PCBP1, BSG, ARHGAP1, BZW1, BZW2, DBN1, β-actin, Nestin, CD133, GAPDH, and CD44 see Table S1	Tsingke	N/A
Recombinant DNA		
pLKO-shCtrl	This paper	N/A
pLKO-shCD97-1	This paper	N/A
pLKO-shCD97-3	This paper	N/A
pCDH-EF1-copGFP-T2A-Puro	Addgene Kazuhiro Oka Lab Materials	Addgene plasmid #72263
pCDH-GFP-CD97	This paper	N/A
pCDH-GFP-BZW1	This paper	N/A
pCDH-GFP-BZW2	This paper	N/A
pCDH-GFP-ARHGAP1	This paper	N/A
pCDH-GFP-hCD97 CAR	This paper	N/A
pCDH-GFP-mCD97 CAR	This paper	N/A
LentiCRISPRv2GFP-sgCtrl	This paper	N/A
LentiCRISPRv2GFP-SgCD97-1	This paper	N/A
LentiCRISPRv2GFP-SgCD97-2	This paper	N/A
Software and algorithms		
Harmony™ software	PerkinElmer Inc.	https://www.perkinelmer.com.cn/
LightCycler 480 software	Roche	https://lifescience.roche.com/
FlowJo software v10.4	FlowJo	https://www.flowjo.com
Microsoft Excel	Microsoft	https://www.microsoft.com/zhcn/microsoft-365/microsoft-office
GraphPad PRISM v8 software	Graphpad	https://www.graphpad.com/
Extreme Limiting Dilution Analysis (ELDA) software	WEHI	http://bioinf.wehi.edu.au/software/elda/
Para Vision v5.1 software	Bruker	https://www.bruker.com/zh.html
Living Image software	Caliper Life Sciences	www.caliperls.com
FastQC (v0.11.7)	Babraham Bioinformatics	https://www.bioinformatics.babraham.ac.uk/projects/fastqc/
Bowtie2 aligner (v2.3.4.1)	Bowtie 2	https://bowtie-bio.sourceforge.net/bowtie2/index.shtml
StringTie (v2.1.3b)	Center For Computational Biology	https://ccb.jhu.edu/software/stringtie/
LPEseq package (v0.99.5)	BioInformatics and BioStatistics	http://statgen.snu.ac.kr/2024/03/06/lpeseq/
DAVID (v6.8)	National Institutes of Health	https://david.ncifcrf.gov/tools.jsp
GenePattern	GenePattern	https://www.genepattern.org/
ZEN Microscopy Software	Zeiss	https://www.zeiss.com.cn/
Adobe Photoshop	Adobe	https://www.adobe.com/cn/products/photoshop.html
Social Sciences software (v16)	IBM SPSS Statistics	https://www.ibm.com/products/spss-statistics
CytExpert software v1.0	Beckman	https://www.beckman.com/flow-cytometry/research-flow-cytometers/cytoflex/software
Other		
PVDF membranes	Millipore	Cat# IPVH00010

(*Continued on next page*)

Continued

REAGENT or RESOURCE	SOURCE	IDENTIFIER
Amersham ECL Prime western blotting detection reagent	Cytiva Lifescience	Cat# RPN2232
96-well plates	Falcon®	Cat# 3300
96-well black plates	LABSELECT	Cat# 31112
BD LypoplateTM Screening Panels	BD Biosciences	Cat# 560747

EXPERIMENTAL MODEL AND SUBJECT DETAILS

Cell lines and cell culture

83, X01, 528, 131, 448, and GSC772 GSCs were obtained as described in our previous reports.[79,80] GSC428 was generously provided by Professor Xun Jin of the Tianjin Medical University Cancer Institute and Hospital. GSC211, GSC924, and GSC028 GSCs were newly isolated using Patel's method.[81] GBM specimens were collected from patients after obtaining informed written consent and approval from the Ethics Committees at Henan Provincial People's Hospital (Henan, China, #2020-107). All GSCs were authenticated by STR testing and maintained in DMEM/F-12 (Gibco) supplemented with B27 (Invitrogen), EGF (10 ng/mL, R&D Systems), and bFGF (5 ng/mL for X01, 448, 131, and 83; 10 ng/mL for GSC772). Human HA1800 astrocytes were purchased from ScienCell Research Laboratory. U87 and 293T cells were purchased from the American Type Culture Collection (ATCC). U251 cells were purchased from Cellosaurus and GL261 cells were obtained from Neuros Creative Biolabs. The cells were maintained in high-glucose DMEM (HyClone) supplemented with 10% fetal bovine serum (FBS; HyClone), 1% Penicillin-Streptomycin (P/S; Gibco), and 1% NEAA Cell Culture Additive (Oricellbio). X01-Luc, 83-Luc, GL261-Luc, and U87-Luc cells were transduced with a luciferase-expressing vector for *in vivo* monitoring and coculture experiments with CAR T cells. All cell cultures were incubated at 37°C in a humidified incubator with 5% CO_2 and repeatedly screened for mycoplasma.

In vivo animal model

All animal experiments were conducted in accordance with protocols approved by the Institutional Animal Care and Use Committee of the National Cancer Center, Republic of Korea, and the Animal Care and Use Committee of Laboratory Animal Center, Henan University (HUSOM2020-018). BALB/c nude mice were purchased from Orient Bio (Korea) and SiPeiFu (SPF) (Beijing) Biotechnology Co., Ltd. (China)], and NTG mice were purchased from SiPeiFu (SPF) (Beijing) Biotechnology Co., Ltd. The animals were group-housed in ventilated cages under controlled temperature and humidity with a 12 h light-dark cycle. Every animal was randomized by body weight before the experiments. For the orthotopic mouse model,[79,80] GSCs were first resuspended in DMEM/F-12 supplemented with B27, EGF (10 ng/mL), and bFGF (5 ng/mL), and then transplanted into the left striatum of BALB/c nude mice by stereotactic injection. The injection coordinates were 2.2 mm to the left of the midline and 0.2 mm posterior to the bregma at a depth of 3.5 mm. The brain of each mouse was harvested and fixed with 4% PFA. All mice used in this study were 5-week-old female mice, assigned to groups randomly. Female animals were involved, and sex was not considered as a biological variable.

Human GBM tissue and healthy blood samples

Peripheral blood mononuclear cells (PBMCs) were isolated from fresh blood samples of healthy donors (n = 3), and GBM specimens for GSCs isolation were collected from patients after obtaining informed written consent and approval from the Ethics Committees at Henan Provincial People's Hospital (Henan, China, #2020-107).

METHOD DETAILS

Screening of cell-surface markers

Cell surface markers on GSCs were screened using a panel of monoclonal antibodies against human cell surface markers (BD Lypoplate Screening Panels, BD Biosciences). Astrocytes, 83, and X01 cells (5×10^3 cells) were plated in Falcon 96-well imaging plates (GSCs were seeded into wells that had been precoated with laminin overnight). The medium was changed the next day, as indicated in the cell culture method (X01-Diff was changed with 10% FBS containing GSC media), followed by 3 days of culture. The cells were then incubated with primary and secondary antibodies with intermediate washing steps according to the manufacturer's instructions. Fluorescence images were obtained and analyzed using an Operetta CLS microscope (PerkinElmer Inc.) and Harmony software (PerkinElmer Inc.).

Lentivirus production and infection

All shRNA vectors to deplete endogenous human CD97 were purchased from Merck. To generate the lentiviral shRNA construct against human CD97, the following sequences were cloned into the pLKO-lentiviral vectors (shCtrl, 5′-CCTAAGGTTAAGTCGC CCTCG-3'; shCD97-1, 5′-GCCGAACTGGAGGAGATATAT-3'; shCD97-3, 5′-GCGATCCTTATGGCTCATTAT-3′). The lentiviral sgRNA

construct against human CD97, the following sequences were cloned into the LentiCRISPRv2GFP[78] vectors (sgCtrl, 5′-CGAATATT ATTTCTATCGGG-3'; sgCD97-1, 5′-CCTTACCTGGATGGTGACCT-3'; sgCD97-2, 5′-CTCCAAGACAAGCTCAGCCG-3). For the generation of the pCDH-GFP-BZW1 and pCDH-GFP-CD97 constructs for the lentiviral transduction, pCDH-GFP (MiaolingBio) was used, and PCR was performed with the following oligomers: PCR amplified oligomers were as follows: BZW1, sense 5′- ATAGA AGATTCTAGAGCTAGCATGAATAATCAAAAGCAGCAAAAGC-3′ and antisense 5′-GATCGCAGATCCTTCGCGGCCGCTCAGTCA CCTTCTTCAGCTTCAGA-3′, BZW2, sense 5′-CGGCTAGCCGATGGATCCGCTCTCAGAGCT-3′ and antisense 5′- GCGGCCGCAG GTTCAGAGCCCGCT-3′, ARHGAP1, sense 5′-GGCTAGCCATGAATAAGCATCAGAAGCC-3′ and antisense 5′- GCGGCCGCTTAAT TTTCCTCACCTTCCG-3′, CD97, sense 5′-GCTAGCCATGGGAGGCCGCGTCTTTCT-3′ and antisense 5′- TTGCGGCCGCAAAGCG TAATCTGGAACATCGTATGGGTATCATATGCCGGACTCTGATG-3'. All oligomers were purchased from Tsingke. All constructs were verified by DNA sequencing (Tsingke). Lentiviruses were produced as previously reported.[80,82] Briefly, 3.5 × 10^6 293T cells were plated on 100 mm culture dishes and incubated for 24 h before transfection. Then, 4.5 μg of lentiviral constructs (pLKO-shCtrl, pLKO-shCD97-1, pLKO-shCD97-3, pCDH-GFP-BZW1, and pCDH-GFP-CD97), 3 μg of psPAX2 (Addgene), and 1.5 μg of pMD2.G (Addgene) were cotransfected with 27 μL of Lipofectamine 2000 (Invitrogen). The medium was changed 6 h after transfection, and the medium containing lentivirus was harvested at 48 h after transfection. The viral particles were concentrated and purified using a Lenti-X concentrator (Clontech Laboratory). Cells were infected with the lentivirus in the presence of 6 μg/mL polybrene.

Quantitative reverse transcription-polymerase chain reaction (RT-qPCR)

Total RNA was extracted from cells using a RNeasy Mini Kit (QIAGEN, MD, USA) according to the manufacturer's instructions. Total RNA (1 μg) was used as a template to synthesize cDNAs using an Ampigene cDNA Synthesis Kit (Enzo Biochem). RT-qPCR analysis was performed with a Roche Light Cycler 480 Instrument using Ampigene qPCR Green Mix Hi-ROX (Enzo Biochem). The results were analyzed with LightCycler 480 software (Roche). The expression levels of the target genes were normalized to that of β-actin or Vinculin. The following PCR primers were used: CD97 (sense 5′-AGAGCGAGAACACCTGTCAA-3′ and antisense 5′-TCCACATCTGTG CAGACCTT-3′), PCBP1 (sense 5′-CGGCTTCTTATGCACGGAAA-3′ and antisense 5′- TTCCTCCAGCTTGTCGATGA-3′), BSG (sense 5′-AGTACTCCTGCGTCTTCCTC-3′ and antisense 5′-GACGACTTCACAGCCTTCAC-3′), ARHGAP1 (sense 5′-TACCAGGTGCTTC GTTTCCT-3′ and antisense 5′-TGGTGAAGGTGTTGATGGGA-3′), BZW1 (sense 5′-AACAGATGTCCCGTGGTGAT-3′ and antisense 5′-TTGCTCTGCTACAAGCTCCT-3′), BZW2 (sense 5′-TGCCAACTCTGTTACCTCGT-3′ and antisense 5′-AAGCTCCTTAAGACCTG CGT-3′), DBN1 (sense 5′-ATGAGAGGCTCAGGTTCGAG-3′ and antisense 5′-TCATCCCGATGGTCACCAAA-3′), β-actin (sense 5′-GAGGCACTCTTCCAGCCTTC-3′ and antisense 5′-GGATGTCCACGTCACACTTC -3′), GAPDH (sense 5′-GGAGTCCACTGGCG TCTTCAC-3′ and antisense 5′-GAGGCATTGCTGATGATCTTGAGG-3′), Nestin (sense 5′-AAGTCTGCGGGACAAGAGAA-3′ and antisense 5′-TCCACAGACTCCAGTGGTTC-3′), CD133 (sense 5′-GAAAGTGGCATCGTGCAAAC-3′ and antisense 5′-GTACACGTCC TCCGAATCCA-3′), and CD44 (sense 5′-AGCACCATTTCAACCACACC-3′ and antisense 5′-CGGATTTGAATGGCTTGGGT-3′).

Immunoblot analysis (IB)

Proteins were extracted with RIPA buffer supplemented with complete protease inhibitors (Solarbio), separated by electrophoresis, transferred to PVDF membranes (Bio-Rad), and blocked with 5% skim milk (Epizyme Biomedical Technology Co., Ltd.). The membranes were incubated with primary antibodies against CD97 (Abcam), Nestin (BD Transduction Laboratories), Oct3/4 (Proteintech), Nanog (Sangon biotech), p-S6K S371 (Cell Signaling Technology), p-S6K T389 (Cell Signaling Technology), S6K (Cell Signaling Technology), *p*-AKT T308 (Cell Signaling Technology), *p*-AKT S473 (Cell Signaling Technology), AKT (Cell Signaling Technology), ARHGAP1 (Santa Cruz), BZW1 (GeneTex), BZW2 (Bethyl Laboratories), CD133 (Proteintech), CD44 (R&D Systems), SOX2 (R&D Systems), Vinculin (Sigma-Aldrich), and β-actin (Bioworld Technology) overnight at 4°C. The immunoreactive bands were visualized using peroxidase-labeled affinity purified secondary antibodies (KPL) and the Amersham ECL Prime western blotting detection reagent (Cytiva Lifescience).

Flow cytometry

Cells were isolated with Accutase (for GSCs, Sigma-Aldrich) or 0.25% trypsin-EDTA (for adherent cells, Gibco) and washed once with PBS. The cells were stained with anti-human CD97 (PE, BioLegend), anti-human Nestin (APC, Thermofisher), anti-human Oct3/4 (Alexa Fluor 647, BioLegend), anti-human Nanog (Alexa Fluor 647, BioLegend), anti-human CD133 (APC, BioLegend), anti-human CD44 (Alexa Fluor 488, BioLegend), and anti-human CD15 (Alexa Fluor 488, BioLegend) antibodies at 4°C for 20 min. Anti-human/mouse CD49f (APC, BioLegend) and anti-human CD97 (PE, BioLegend) antibodies were added before $CD97^{high}$ GSC sorting. For each cell line, a corresponding negative control was utilized at the time of sample collection. For experiments to detect cytotoxicity, anti-human CD3 (APC, BD Biosciences), anti-human CD4 (PerCP/Cyanine5.5, BioLegend), INF-ϒ (APC, BD Biosciences) or anti-human CD107a (PE, BioLegend) antibodies at 4°C for 20 min. Data were acquired using a BD FACSCalibur and BD LSRFortessa. The cells were sorted using a BD FACSAria III SORP cell sorter. The data were analyzed using FlowJo software v10.4.

PI staining and annexin V staining

Cellular apoptosis was assessed using propidium iodide (PI, BD) staining and Annexin V (Themo Fisher) staining. The cultured GSCs were washed with phosphate-buffered saline (PBS), and resuspended in binding buffer. Subsequently, cells were stained with Annexin V-FITC and PI according to the manufacturer's protocol. The stained cells were then analyzed using flow cytometry.

Cell proliferation assays

GSCs were plated at a density of 1 × 10^3 cells/well in 96-well plates containing DMEM/F-12 supplemented with B27, EGF (10 ng/mL), and bFGF (5 ng/mL) for *in vitro* proliferation assays. The luminescence of viable cells was detected using a CCK-8 Cell Proliferation and Cytotoxicity Assay Kit according to the manufacturer's protocol. The CCK-8 Cell Proliferation and Cytotoxicity Assay is a homogeneous method for determining the number of viable cells in culture based on the quantitation of the amount of dehydrogenase in the mitochondria of viable cells present, which indicates the presence of metabolically active cells. The luminescence signal was detected using a SpectraMax Microplate Reader (Molecular Device) according to the manufacturer's protocol. The results were analyzed and visualized using Microsoft Excel 2016 and GraphPad PRISM v8 software.

LDAs

For *in vitro* LDAs, GSCs were plated at decreasing densities (100, 50, 25, and 5 cells/well) in 96-well plates containing DMEM/F-12 supplemented with B27, EGF (10 ng/mL), and bFGF (5 ng/mL). The LDAs results were processed after 7 to 10 days using Extreme Limiting Dilution Analysis (ELDA) software, which is available at http://bioinf.wehi.edu.au/software/elda/.

Inhibitor treatment

GSCs were plated at a density of 6 × 10^5 cells/well densities in 60 mm culture dishes and incubated with DMEM/F-12 supplemented with B27, EGF (10 ng/mL), and bFGF (5 ng/mL) containing Torin1 (50 and 100 nM, for 48 h; SelleckChem, Houston, TX, USA), AKT inhibitor IV (10 and 20 μM, for 24 h; Cruz Credit, Santa Cruz, CA, USA), Rapamycin (5 and 10 nM, for 24 h; SelleckChem), and JR-AB2-011 (10 and 20 μM, for 48 h; MedChemExpress, Monmouth Junction, NJ, USA). GSCs were collected, and IB was performed as described above.

GSCs were plated in 96-well plates at 10^3 cells/well densities for *in vitro* proliferation assays and at decreasing densities (100, 50, 25, and 5 cells/well) for LDAs. The GSCs were incubated with Torin1 (50 and 100 nM, for 4 days), AKT inhibitor IV (10 and 20 μM, for 3 days), Rapamycin (5 and 10 nM, for 4 days), and JR-AB2-011 (10 and 20 μM, for 6 days) and analyzed as described above.

Mice models

To observe the characteristics of CD97 *in vivo*, sorted $CD97^{high}$ and $CD97^{-/low}$ GSC772 cells (1 × 10^5) were orthotopically injected into the brains of BALB/c nude mice, as mentioned above. Animals were monitored by using magnetic resonance imaging (MRI). All MRI examinations were performed using a high-field 7.0 Tesla Bruker BioSpec 70/20 USR (Bruker) and analyzed using Para Vision v5.1 software (Bruker) as described in a previous report.[79]

To examine the pharmacological effects of JR-AB2-011 *in vivo*, X01-Luc cells (1 × 10^5) were orthotopically injected into the brain of BALB/c nude mice, as mentioned above. Thirteen days after intracranial tumor injection, the mice were daily intraperitoneally (i.p.) injected with JR-AB2-011 (4 mg/kg) or vehicle (45% PEG-300, TOP SCIENCE; 5% DMSO, Sigma-Aldrich; and 5% Tween-80, Sangon Biotech in PBS) for 10 days.

To assess CD97-CAR Th9 cell antitumor activity *in vivo,* X01-Luc cells (1 × 10^5) were orthotopically injected into the brains of NTG mice, as mentioned above. On day 4 after the intracranial tumor injection, CD97-CAR Th9 or Ctrl-CAR Th9 cells (1.5 × 10^6) in 8 μL total volume were stereotactically injected into the brain of mice using the following co-ordinates: the injection coordinates were 2.2 mm to the left of the midline and 0.2 mm posterior to the bregma at a depth of 3.5 mm. In addition, treatment with tail intravenous administration of CD97-CAR Th9 or Ctrl-CAR Th9 cells was administered intravenously on days 4 and 17 after intracranial tumor injection (1× 10^7).

The mice were monitored by detecting bioluminescence using the IVIS Lumina XRMS Series III system (PerkinElmer). The photons emitted from the luciferase-expressing tumor cells were quantified using Living Image software (Caliper Life Sciences). A pseudocolor image representing light intensity (blue = least intense and red = most intense) was generated and superimposed over the grayscale reference image. The animals were imaged twice weekly beginning a week after the injection. Mice were euthanized when they met euthanasia criteria (neurological deficits, 20% weight loss, and signs of distress). Survival was analyzed using GraphPad PRISM v8 software.

Immunofluorescence (IF) staining

For histological observations, the brains were removed, fixed with 4% paraformaldehyde for 24 h at 4°C, sectioned at a thickness of 4 μm using an essential microtome (Leica RM2125 RTS), and then subjected to an antigen retrieval process using citrate buffer (pH 6.0). Sections were immunostained overnight at 4°C in a humidified chamber with primary antibodies against CD97 (Abcam), Nestin (BD Transduction Laboratories), ARHGAP1 (Santa Cruz), BZW1 (GeneTex), and BZW2 (Bethyl Laboratories) that had been diluted to the working concentration with antibody diluent buffer (IHC World). Immunoreactive proteins were visualized with the appropriate fluorescent secondary antibodies [Alexa Fluor 488-*anti*-rabbit IgG (Thermo Fisher Scientific); Alexa Fluor 568 anti-mouse IgG (Thermo Fisher Scientific)]. The nuclei were stained with 4′,6-diamidino-2-phenylindole (DAPI, Thermo-Fisher Scientific), and fluorescence images were captured using a Zeiss LSM 780 Confocal Laser Scanning Microscope (Carl Zeiss).

Bioinformatics analysis

The mRNA expression of CD97 and other stemness markers in Restall[40] and Rechards[41] scRNA-Seq cohorts were analyzed using Single Cell Portal (https://singlecell.broadinstitute.org/single_cell).

For the analysis of mRNA expression and survival prognosis, CD97, PCBP1, BSG, ARHGAP1, BZW2, BZW1, and DBN1 mRNA expression and clinical phenotypes were obtained from GBM microarray data in TCGA[83,84] (UCSC Xena portal, https://xena.ucsc.edu/public), CGGA[85] and REMBRANDT[86] (CGGA portal, http://www.cgga.org.cn) databases. All statistical analyses, evaluations of gene expression, and Kaplan–Meier estimations were performed using GraphPad PRISM v8 software.

Analysis of RNA-sequencing data

RNA-seq libraries were prepared using a TruSeq Stranded mRNA LT Sample Prep kit (Illumina) and were sent for transcriptome resequencing. The phred quality score of the obtained raw FASTQ files was checked using FastQC (v0.11.7). The sequences were mapped onto the GRCh37 human genome using Bowtie2 aligner (v2.3.4.1) and further assembled potential transcript using StringTie (v2.1.3b). For the identification of differentially expressed genes (DEGs), read counts were normalized and quantified using the LPEseq package (v0.99.5), which is designed for nonreplicated samples. Genes with statistical significance (p value and Q value with <0.01) and a fold change ±2.0 were chosen as significant DEGs. Gene Ontology (GO) analysis of downregulated genes in CD97 knockdown GSCs was performed using DAVID (v6.8). GSEA (v4.2) of the hallmark genes was performed using GenePattern.

CAR T cell manufacturing and transduction

PBMCs were isolated from healthy donors, separated by density gradient centrifugation (Ficoll-Paque plus; GE Healthcare), and then cultured with RPMI-1640 (ATCC) supplemented with 10% FBS (HyClone) and 1% P/S (Gibco). $CD4^+$ T cells were prepared by purifying $CD4^+$ T cells from PBMCs using an EasySep Human $CD4^+$ T cell Isolation Kit (STEMCELL Technologies Inc.), followed by activation and polarization into Th9 cells. T cells were activated using two factors: CD3 (1 μg/mL) (BD Biosciences) and CD28 (2 μg/mL) (BD Biosciences). The Th9-polarizing medium was RPMI-1640 medium supplemented with hIL-4 (10 ng/mL, Novoprotein Scientific Inc.), hTGF-β1 (1 ng/mL, Novoprotein Scientific Inc.), and *InVivo*MAb anti-human-IFN-γ (10 μg/mL, BioXcell) and was incubated with cells for 5 days. The polarized T cell population underwent lentiviral transduction to express a second-generation anti-CD97 CAR and Ctrl vector. Blood samples were collected from healthy donors after obtaining informed written consent and approval from the Ethics Committees at Henan University (HUSOM2020-018).

Generation of murine CAR-T cells

Murine $CD3^+$ T cells were purified from C57BL/6J mice splenocytes using the EasySep Mouse T cell Isolation Kit (STEMCELL Technologies Inc.) and stimulated on plates coated with 2 μg/mL mCD3ε (BD Pharmingen) and 2 μg/mL mCD28 mAbs (Biolegend) for 48 h. The stimulated T cell population underwent lentiviral transduction to express a second-generation anti-CD97 CAR T cells were expanded in complete medium RPMI-1640 (ATCC), 10% FBS (Hyclone), 1% Penicillin-Streptomycin (Gibco) with hIL-2 (10 ng/mL; PeproTech.) changing medium every 2 days. On days 6–7, T cells were collected and used for functional assays *in vitro* and *in vivo*.

To assess CD97-CAR T cell antitumor activity *in vivo*, Gl261-Luc-CD97 expression cells (1×10^5) were orthotopically injected into the brains of C57BL/6J mice, as mentioned above. On day 4 after the intracranial tumor injection, CD97-CAR T or Untreated T cells (1×10^6) in 8 μL total volume were stereotactically injected into the brain of mice using the following co-ordinates: the injection co-ordinates were 2.2 mm to the left of the midline and 0.2 mm posterior to the bregma at a depth of 3.5 mm.

Fluorescence assay of viable cells

CD97-CAR Th9 or Ctrl-CAR Th9 cells were used as effectors (E), and human GSCs or GBM cell lines were used as targets (T) and were previously transduced with luciferase lentiviral vectors. The viability of target cells at different effector-to-target ratios (E:T) was evaluated in 96-well black plates (LABSELECT) using a Spectra Max ID3 Multifunctional Enzyme Labeler (Molecular Devices). Cultures containing the medium alone were used as controls, representing 100% and 0% cell viability, respectively. The average viability was calculated as 100 × (experimental cell fluorescence −0% viable cell fluorescence)/(100% viable cell fluorescence −0% viable cell fluorescence).

Cytotoxicity assay

For analysis of the CAR-expressing T cell killing effect, target cells (GSCs and non-GSCs) were incubated with Celltracker CM-DiI dye (1:1000; Yeasen) at 37°C for 5 min and then incubated at 4°C for 15 min to terminate the staining and washed with PBS and co-cultured with Ctrl-CAR Th9 cells or CD97-CAR Th9 cells in confocal live cell culture dishes. The fluorescence images were captured using a Zeiss LSM 780 Confocal Laser Scanning Microscope.

Isolation of tumor-infiltrating immune cells

Brains were harvested from X01-Luc xenografts on days 2 and 7 after injection of CD97-CAR T cells, followed by enzymatic dissociation, and filtered through a 40 μm cell strainer. The samples were stained with anti-human CD3 antibody (APC, BioLegend), anti-human CD4

antibody (PerCP/Cyanine5.5, BioLegend), and anti-human CD107a antibody (PE, BioLegend) at 4°C for 20 min. Data were acquired using a CytoFLEX (Beckman Coulter, Inc.) and analyzed using CytExpert software v1.0.

QUANTIFICATION AND STATISTICAL ANALYSIS

The Kaplan–Meier method was used to plot survival curves. For patients who were alive at the time of the last follow-up, survival records were censored in our analysis. The Statistical Package for the Social Sciences software (v16) was used for statistical analyses. In mouse experiments, the results from multiple datasets were compared using analysis of variance (ANOVA) and the log rank (Mantel–Cox) test. The results from experiments assessing two datasets were compared using a two-tailed Student's t test (in the cases where the samples are independent and follow a normal distribution). If the data doesn't follow a normal distribution, the Mann-Whitney U test should be conducted instead. p values <0.05 were considered to indicate statistical significance; individual p values are provided in the figure legends. Three technical replicates were performed for all experiments for reproducibility.